Properties and mechanisms of scintillation in $CsGd_2F_7:Ce^{3+}$ and $CsY_2F_7:Ce^{3+}$ crystals

1995 J. Phys.: Condens. Matter 7 3063

(http://iopscience.iop.org/0953-8984/7/15/013)

J. Phys.: Condens. Matter 7 (1995) 3063–3088. Printed in the UK

Properties and mechanisms of scintillation in $CsGd_2F_7:Ce^{3+}$ and $CsY_2F_7:Ce^{3+}$ crystals

D R Schaart†, P Dorenbos†, C W E van Eijk†, R Visser†, C Pedrini‡, B Moine‡ and N M Khaidukov§

† Delft University of Technology, Faculty of Applied Physics, c/o IRI, Mekelweg 15, 2629 JB Delft, The Netherlands

‡ Universite Lyon I, Batiment 205, 43 Boulevard du 11 Novembre 1918, 69622 Villeurbanne Cédex, France

§ N S Kurnakov Institute of General and Inorganic Chemistry, Leninskii Prospect 31, 117907 Moscow, Russia

Received 22 December 1994

Abstract. The scintillation properties of Ce^{3+} doped $CsGd_2F_7$ and CsY_2F_7 crystals have been studied at various temperatures. Upon x-ray excitation CsY_2F_7: 5 mol% Ce^{3+} shows fast ($\tau \approx 32$ ns) Ce^{3+} $5d \rightarrow 4f$ luminescence with a yield of 1400 photons MeV^{-1} at room temperature. The most intense Ce^{3+} luminescence of about 7300 photons MeV^{-1} is found in $CsGd_2F_7$: 20 mol% Ce^{3+}. The scintillation decay curve of $CsGd_2F_7:Ce^{3+}$ consists of at least two non-exponential components, one of the order of tens of nanoseconds and one in the microsecond region. Both CsY_2F_7 and $CsGd_2F_7$ show a broad STE emission band at around 445 nm, especially at low temperatures. VUV photon excitation measurements at 300 K and low temperatures revealed the presence of two inequivalent types of Ce^{3+} centres in both CsY_2F_7 and $CsGd_2F_7$. The presence of Gd^{3+} appears to have a dominating influence on the luminescence characteristics of $CsGd_2F_7:Ce^{3+}$, due to the occurrence of both $Ce^{3+} \rightarrow Gd^{3+}$ and $Gd^{3+} \rightarrow Ce^{3+}$ energy transfer as well as energy migration over the Gd^{3+} sublattice. On the basis of the optical studies, models of the scintillation mechanisms of CsY_2F_7 and $CsGd_2F_7$ are developed which account for the scintillation properties of these crystals.

1. Introduction

The Ce^{3+} ion is one of the most promising rare-earth ions for prospective use as a luminescence dopant in inorganic scintillators, due to the relatively small intrinsic decay time of the dipole-allowed $5d \rightarrow 4f$ transition. A number of host lattices are known which show fast luminescence with a high light yield if doped with Ce^{3+}; see, for example, [1] and references therein. Crucial to such a good performance is that the energy created upon absorption of a gamma quantum, which is available as electron–hole pairs, is efficiently transported to the Ce^{3+} ions. Thus knowledge of the processes which are responsible for this transport is of much importance in the search for better scintillators. One of the ways by which such knowledge can be acquired is the systematic investigation of luminescence and energy transfer processes by means of photon excitation experiments. Since the bandgap energy of inorganic scintillators can be as large as 10 eV one should be able to perform these measurements not only in the visible and UV, but also in the VUV (vacuum ultra-violet) region.

In section 3.1 we report on the scintillation properties of isostructural $CsY_2F_7:Ce^{3+}$ and $CsGd_2F_7:Ce^{3+}$. Some of the scintillation properties of $CsGd_2F_7$: 0.1, 0.3, 1, 3, and 10

0953-8984/95/153063+26$19.50

mol% Ce^{3+} have already been reported on [2, 3, 4]. In this work the scintillation properties of $CsGd_2F_7$: 0.004, 20 and 30 mol% are also discussed. In addition samples of CsY_2F_7 doped with 0.08, 0.12, 0.5 and 5 mol% Ce^{3+} are studied and compared with $CsGd_2F_7 : Ce^{3+}$. Both $CsGd_2F_7$ and CsY_2F_7 have an orthorhombic structure [5], with probably eight different sites for the Gd^{3+} (or Y^{3+}) ion [6]. Ce^{3+} ions are expected to enter the crystal at Gd^{3+} (or Y^{3+}) sites. The density of $CsGd_2F_7$ (5.74 g cm^{-3}) is higher than that of CsY_2F_7 (4.53 g cm^{-3}) because of the relatively high atomic number of Gd^{3+}, resulting in a better stopping power for gamma rays.

The optical luminescence properties of the crystals were studied by means of a new VUV excitation set-up which is described in section 2. The results are presented in sections 3.2 and 3.3. The characteristics of the different luminescence centres in the samples are investigated. Furthermore a number of energy-transfer and migration processes are studied and discussed. On the basis of the results of the optical studies, qualitative models of the scintillation mechanisms of $CsY_2F_7 : Ce^{3+}$ and $CsGd_2F_7 : Ce^{3+}$ are suggested.

Finally, in section 4 a simple quantitative model of the scintillation mechanism of $CsGd_2F_7 : Ce^{3+}$ is developed, which correctly predicts many of the scintillation properties of $CsGd_2F_7 : Ce^{3+}$ presented in section 3.1.2

2. Experimental procedures

Cerium-doped CsY_2F_7 and $CsGd_2F_7$ crystals were grown by one of us (Khaidukov), using the hydrothermal synthesis technique. This provided colourless single crystals with many facets. Diameters varied from about two to about ten millimetres. The crystals were not analysed for the content of Ce^{3+} or the presence of unwanted impurities. The reported Ce^{3+} concentrations are calculated from the weighted-in amounts of CeF_3 prior to crystal growth, other than for the 0.004 mol% doped $CsGd_2F_7$ sample and the 0.08 and 0.12 mol% doped CsY_2F_7 samples. For these samples the concentrations were derived from comparison of the absorption spectra to that of $CsGd_2F_7$: 0.1 mol% Ce^{3+}. The crystals used in the experiments were ground and polished to obtain two plane-parallel faces. Thicknesses varied between about one and three millimetres. The optical quality of the crystals was not always good and varied considerably from crystal to crystal. For some Ce^{3+} concentrations relatively clear samples could be obtained, while for other concentrations the samples showed cracks, haziness and/or opaque inclusions.

For details on the set-ups used for the measurement of pulse height, scintillation decay and x-ray emission spectra, refer to [7]. All x-ray emission spectra were corrected for transmittance and second-order transmission of the monochromator as well as the quantum efficiency of the photomultiplier tube (PMT).

To measure optical absorption spectra between 115 and 370 nm, crystals were illuminated with an ARC (Acton Research Corporation) DS-775 deuterium light source. Also, some absorption spectra between 190 and 820 nm were measured by means of a Hewlett–Packard type HP 8452A diode array spectrophotometer. Spectra were recorded using both a parallel beam and diffused light. In the latter experiments a quartz diffuser was placed directly against the sample at the side of the light source. These measurements were used to correct the x-ray emission spectra for transmittance of the crystal as described in section 3.1. Parallel-beam measurements were used to determine the absorption spectra of dopants. All optical absorption spectra were corrected for the spectral shape of the light source and transmittance of the system.

A VUV excitation set-up was used to measure excitation and VUV-excited emission spectra. In this set-up the light of an ARC type DS-775 deuterium light source is passed

through an ARC type VM-502 vacuum monochromator and focused on a sample by means of a MgF_2 lens. The light emitted by the sample is collected by a quartz lens and monitored using a Jobin–Yvon type H10 UV monochromator and a Phillips type XP2020Q photomultiplier tube. The sample and lenses are contained in an evacuated chamber equipped with MgF_2 and quartz entrance and exit windows, respectively. With this set-up excitation and emission spectra can be recorded for 130 nm $\leqslant \lambda_{ex} \leqslant$ 350 nm and 180 nm $\leqslant \lambda_{em} \leqslant$ 540 nm, λ_{ex} and λ_{em} being the excitation and emission wavelengths, respectively. The angle between the incident and emission beams is 90°; the angle between the incident beam and the normal of the sample surface was set to 30°. In order to perform measurements at low temperatures samples were mounted on a copper sample holder cooled by liquid nitrogen. The quantum efficiencies reported in this article are estimations of the external quantum efficiency, defined as the number of emitted photons divided by the number of incident photons. The estimations are based on a comparison of the results on the sample with those obtained from a sodium salicylate reference sample by measurement under nearly identical experimental conditions. The difference in detection efficiency of the emissions from the sample and the reference sample is corrected for. Sodium salicylate is assumed to have a uniform quantum efficiency of 65% at room temperature and 81% at 77 K between 30 and 350 nm [8].

Measurements were also performed using a set-up installed at the SA61 line of the SUPER-ACO synchrotron facility at LURE (Laboratoire pour l'Utilisation du Rayonement) in Orsay, France. Excitation spectra, at room temperature and about 40 K, were recorded between 30 and 300 nm using sodium salicylate as a reference. VUV-excited luminescence decay spectra could be recorded for $t < 120$ ns at room temperature.

3. Results and discussion

3.1. Scintillation properties

X-ray-excited emission spectra, decay spectra and pulse height spectra—the latter two upon excitation by 662 keV gamma quanta—were measured. Since most of the crystals investigated showed considerable scattering of light, we measured the optical transmission spectra of all crystals using a diffuser as described in section 2. It appeared that the maximum T_0 of the optical transmittance T varied somewhat for different samples. In order to provide a rough correction for these differences we assumed the transmittance of the undoped crystal to be constant and equal to T_0, which is a good approximation in the wavelength region of interest, i.e. at emission wavelengths. The highest value of T_0 found in a clear sample was about 0.80. Using $T = 2n/(n^2 + 1)$ this would mean that the refractive index n of these crystals is about 2, if the loss of light is entirely due to Fresnel reflections. In view of the above assumption, we multiplied all emission spectra by $0.80/T_0$. The emission spectra shown are thus not corrected for Ce^{3+} self-absorption.

3.1.1. $CsY_2F_7:Ce^{3+}$. In figure 1 the emission spectra at room temperature of CsY_2F_7 doped with 0.12, 0.5 and 5 mol% Ce^{3+} are shown. The spectrum of CsY_2F_7 : 5 mol% Ce^{3+} consists of a broad Ce^{3+} 5d $\rightarrow$ 4f emission band with a maximum at 333 nm. The spectrum of CsY_2F_7 : 0.5 mol% Ce^{3+} shows a Ce^{3+} emission band too, but the maximum is now at about 325 nm. This band extends somewhat more to the short-wavelength side. In addition to this band, a line at 312 nm is visible, which can be identified as Gd^{3+} $^6P_{3/2} \rightarrow {}^8S_{7/2}$ emission, caused by the presence of Gd^{3+} impurities. The spectrum of the 0.12 mol% doped sample shows the same Gd^{3+} line. The maximum of the Ce^{3+} emission in this sample is

at about 315 nm. The broadening towards short wavelengths is even more pronounced, but also a new structure is visible at longer wavelengths.

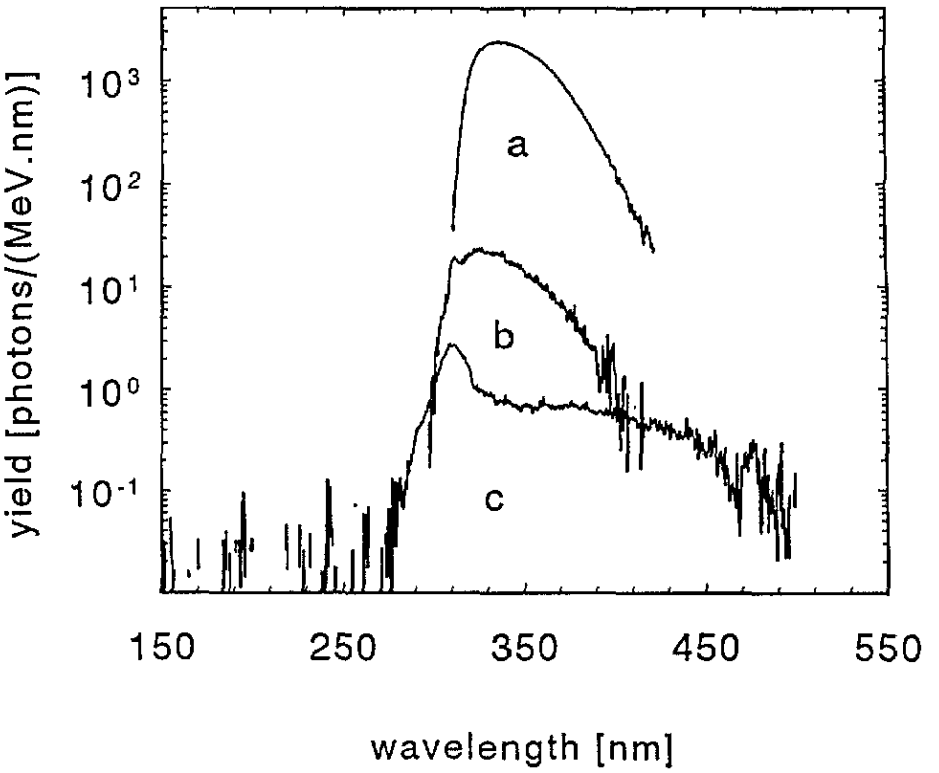

Figure 1. X-ray-induced emission spectra of (a) 2.15 mm thick CsY_2F_7 : 5 mol% Ce^{3+}, (b) 2.1 mm thick CsY_2F_7 : 0.5 mol% Ce^{3+}, (c) 1.5 mm thick CsY_2F_7 : 0.12 mol% Ce^{3+}. The wavelength resolutions are (a) and (b) 4 nm and (c) 12 nm. For clarity, the spectra (a) and (b) have been multiplied by 100 and 10, respectively.

It will be shown that the Ce^{3+} emission band in these spectra can in fact be described as a weighted sum of two Ce^{3+} emission bands with maxima at 310 nm and 333 nm which originate from two types of Ce^{3+} centre, which we will call Ce_1^{3+} and Ce_2^{3+} respectively. In crystals doped with more than a few mol% Ce^{3+}, only the second one is visible due to $Ce_1^{3+} \rightarrow Ce_2^{3+}$ energy transfer. We will also show that the broad emission band at longer wavelengths can be ascribed to self-trapped exciton (STE) luminescence.

The total light yields of the Ce^{3+} emission for different Ce^{3+} concentrations as derived from these spectra are listed in table 1. The 5 mol% doped sample shows a yield of about 1400 photons MeV^{-1} and it seems likely that a higher Ce^{3+} concentration will result in a higher yield.

The x-ray emission spectra of CsY_2F_7 : 0.08 mol% Ce^{3+} have been recorded at different temperatures between 95 and 300 K. Two of these are shown in figure 2. Again, these spectra can be composed of the Ce^{3+}, Gd^{3+} and STE bands described above. Figure 3 shows the absolute yield of the STE luminescence as a function of temperature, as derived from the spectra. Note that the STE emission is hardly visible at 300 K in this sample, while the Ce^{3+} yield is much higher than in the 0.12 mol% doped sample. In the latter sample the STE luminescence is in fact extraordinarily strong at room temperature, compared to

Table 1. Some experimental data concerning the scintillation properties of $CsGd_2F_7:Ce^{3+}$ and $CsY_2F_7:Ce^{3+}$.

Host	Ce concentration (mol%)	Light yield[a] (photons MeV^{-1})	Decay constant[b] τ_f^d (ns)	Decay constant[b] τ_s (μs)	Photoelectron yield[b,c] (photoelectrons MeV^{-1})	$\Delta E/E$[b,c] (%)
$CsGd_2F_7$	30	6100 ± 600	25 ± 25	2 ± 1		
	20	7300 ± 700	20 ± 5 (22%)	3 ± 1		
	10	6200 ± 600	25 ± 15 (13%)	7 ± 4	1130	13.5
	3	2900 ± 600	25 ± 20 (1.5%)	22 ± 10	380	24
	1	2000 ± 300				
	0.3	900 ± 300				
	0.1	290 ± 100				
	0.004	9 ± 4				
CsY_2F_7	5	1400 ± 300	32 ± 1 (100%)			
	0.5	190 ± 60				
	0.12	55 ± 20				
	0.08	260 ± 100				

[a] Upon x-ray excitation.

[b] Upon 662 keV gamma excitation. In the case of $CsGd_2F_7:30$ mol% Ce^{3+}, measurements were performed using a LeCroy digital oscilloscope. All other measurements were performed using a single-photon-counting technique. In these cases, since the decay of both fast and slow components deviate from exponentiality, estimates for the decay rates are given as a mean between the values at the beginning and the end of the decay curve. The difference between the extrema and the mean is indicated by the error margins.

[c] Measured with a shaping time of 8 μs and an Phillips XP2020Q PMT.

[d] The percentage of the total Ce^{3+} light yield originating from the fast component is indicated between parentheses.

the other CsY_2F_7 and $CsGd_2F_7$ samples we investigated. In addition to the Ce^{3+} and STE bands, at low temperatures some luminescence is observed between 200 and 300 nm in $CsY_2F_7:0.08$ mol% Ce^{3+}. We are not sure about the origin of this luminescence, but it might be due to the presence of some impurities, like Gd^{3+} and Pr^{3+}. Note that the spectra shown are not corrected for Ce^{3+} absorption, which is of importance at these wavelengths (see figure 7).

The decay of the scintillation pulse of the 5 mol% doped sample can in the first instance be described as a single exponential with decay constant $\tau \approx 32$ ns (see curve b in figure 11). A more detailed treatment of the decay characteristics will be given in section 3.3.2.

3.1.2. $CsGd_2F_7:Ce^{3+}$. In figure 4 the emission spectra of $CsGd_2F_7:0.004$, 0.1, 1.0 and 10 mol% Ce^{3+} are shown. In all of these spectra, a Ce^{3+} 5d $\rightarrow$ 4f luminescence band with a maximum at 333 nm is observed. Furthermore a Gd^{3+} $^6P_{3/2} \rightarrow {}^8S$ line at 312 nm is visible in the 0.1 and 0.004 mol% doped samples. In the latter, Gd^{3+} $^6I \rightarrow {}^8S$, $^6D \rightarrow {}^8S$ and $^6G \rightarrow {}^8S$ lines are also observed at respectively 280, 253 and 204 nm. Between 350 and 540 nm many lines are visible which probably originate from various rare-earth impurities.

The broadening of the Ce^{3+} emission towards shorter wavelengths at low Ce^{3+} concentrations which was observed in CsY_2F_7 does not occur in these crystals. For Ce^{3+} concentrations of a few mol% and higher however, both CsY_2F_7 and $CsGd_2F_7$ show the same Ce_2^{3+} emission band. It will be shown that, although Ce_1^{3+} centres are also present in $CsGd_2F_7$, the Ce_1^{3+} emission band is not visible due to efficient $Ce_1^{3+} \rightarrow Gd^{3+}$ energy transfer. In table 1 the absolute yields of the Ce^{3+} emission as derived from these spectra are

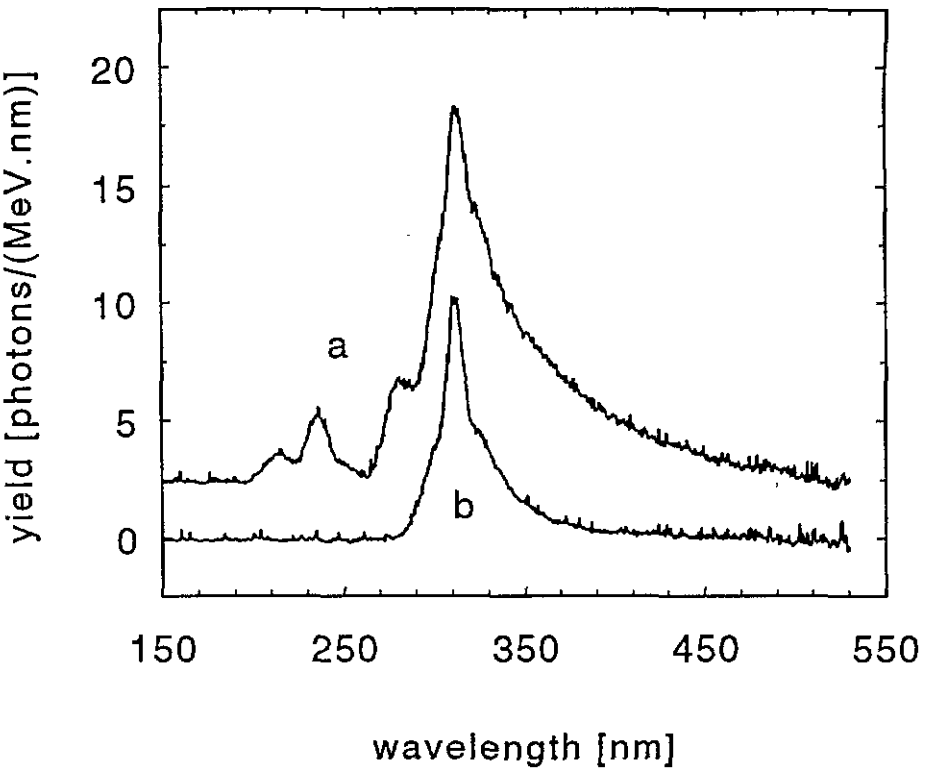

Figure 2. X-ray-induced emission spectra of 1.4 mm thick CsY_2F_7 : 0.08 mol% Ce^{3+} at (a) 95 K and (b) 297 K. The resolution is 8 nm. Spectrum (a) is shifted by 2.5 photons/(MeV·nm) for clarity.

listed for concentrations between 0.004 and 30 mol%. It should be noted that the spectrum of the 0.004 mol% doped sample was not corrected for self-absorption as described above, so the value for this sample is in fact a lower limit. $CsGd_2F_7$: 20 mol% Ce^{3+} shows the highest yield of about 7300 photons MeV^{-1}.

The x-ray-excited emission spectra of $CsGd_2F_7$: 0.004, 0.1 and 10 mol% Ce^{3+} were recorded at temperatures between 95 and 425 K. From these the yields of the Ce^{3+} emission were derived. For $CsGd_2F_7$: 0.004 and 10 mol% Ce^{3+}, the results are shown in figure 5. Again, the values for the 0.004 mol% doped sample are a lower limit. The yield of a 3.1 mm thick sample of $CsGd_2F_7$: 0.1 mol% Ce^{3+} was found to be 290 ± 30 photons MeV^{-1} at 295 K and 570 ± 60 photons MeV^{-1} at 148 K. We note that while the yield of $CsGd_2F_7$: 10 mol% Ce^{3+} is almost independent of temperature between 95 K and room temperature, the yield of $CsGd_2F_7$: 0.004 mol% Ce^{3+} decreases quite strongly with increasing temperature. As the measurements were started at the low-temperature side, we ascribe the sudden increase of the Ce^{3+} yield of the 10 mol% doped sample at 350 K to annealing of radiation damage caused by the preceding measurements at lower temperatures. This assumption is supported by the fact that a slight reddish brown colouring of CsY_2F_7 and $CsGd_2F_7$ crystals was observed after x-ray irradiation at room temperature, which could be removed by heating the crystal. Apart from Ce^{3+} luminescence, a STE emission band similar to that in CsY_2F_7 was also present in $CsGd_2F_7$ crystals. Between 200 and 300 nm no luminescence was observed other than the Gd^{3+} lines mentioned before.

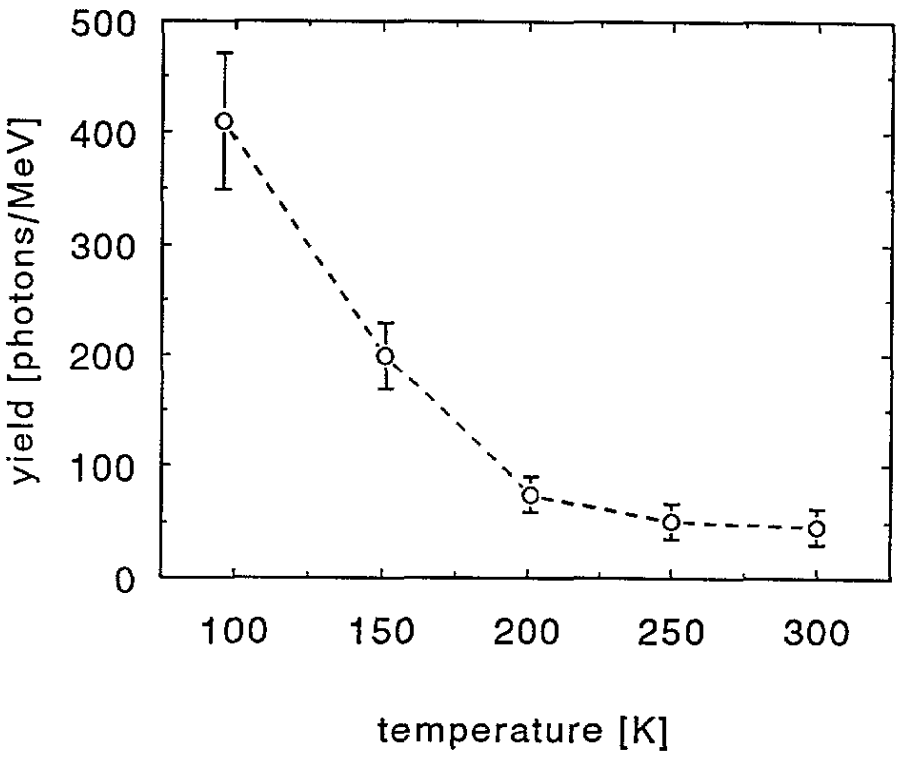

Figure 3. The absorption-corrected integral light yield as a function of temperature of the STE luminescence observed in 1.4 mm thick CsY_2F_7 : 0.08 mol% Ce^{3+}.

The scintillation decay spectra of several of these crystals were measured. The spectra of $CsGd_2F_7$: 3 and 10 mol% are shown in figure 6. Both consist of two non-exponential components, one of the order of tens of nanoseconds, but effectively shorter than the 32 ns exponential decay found in $CsY_2F_7:Ce^{3+}$, and another one in the microsecond region. Estimates for the decay constants τ_f and τ_s of respectively the fast and slow decay component of a number of samples are given in table 1. For the samples doped with 1 mol% Ce^{3+} or less the decay times of the long component were too long and the intensity of the short component too low to be measurable with our set-ups.

Finally the pulse height spectra of some of these crystals were measured using a shaping time of 8 μs. The photoelectron yields and energy resolution (i.e. the full width at half-maximum of the total absorption peak) as derived from these are listed in table 1.

3.2. Optical absorption data

In figure 7 several absorption spectra are shown. In these spectra the absorption coefficient, defined as $\mu \equiv -(1/d)\ln(T/T_0)$, in which d is the crystal thickness, is plotted versus wavelength. In the spectrum of CsY_2F_7 : 0.12 mol% Ce^{3+} one can distinguish at least six different bands at 186, 200, 225, 245, 265 and 295 nm. We found the height of each band to be proportional to the Ce^{3+} concentration, which clearly indicates that these absorptions are all caused by the presence of Ce^{3+}. However, since the point symmetry of the crystal at the rare-earth sites is low, one would expect the fivefold-degenerate 5d levels of Ce^{3+} ions to be split into as many sublevels by the crystal field, giving rise to five distinct absorption

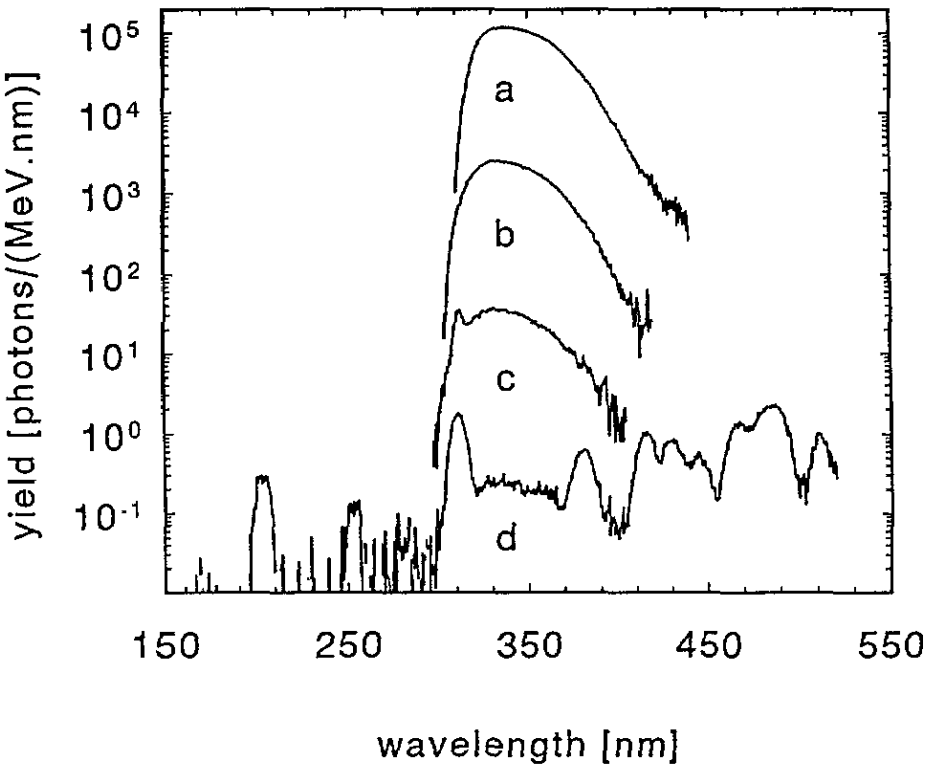

Figure 4. X-ray-induced emission spectra of (a) 1.55 mm thick $CsGd_2F_7$: 10 mol% Ce^{3+}, (b) 2.0 mm thick $CsGd_2F_7$: 1 mol% Ce^{3+}, (c) 1.35 mm thick $CsGd_2F_7$: 0.1 mol% Ce^{3+} and (d) unpolished $CsGd_2F_7$: 0.004 mol% Ce^{3+}. The resolutions are (a), (b) and (c) 4 nm and (d) 8 nm. For clarity, spectra (a), (b) and (c) are multiplied by 1000, 100 and 10, respectively.

bands. The fact that the number of absorption bands is more than five is therefore already an indication that more than one type of Ce^{3+} centre might be present in these crystals.

The spectrum of $CsGd_2F_7$: 0.004 mol% Ce^{3+} shows many Gd^{3+} absorption lines between 171 and 312 nm. The Ce^{3+} absorption bands are visible only very weakly.

Comparison of the spectra of CsY_2F_7 : 0.12 mol% Ce^{3+} and $CsGd_2F_7$: 0.1 mol% Ce^{3+}, in which the Ce^{3+} absorption bands are clearly visible, shows that the positions of these bands are equal in both crystals. This is not unexpected since they have equal crystal structures.

The absorption band at 295 nm is relatively weak in the spectrum of CsY_2F_7 : 0.12 mol% Ce^{3+}, which can be explained as follows. As a result of the broadening of the Ce^{3+} emission band of CsY_2F_7 : Ce^{3+} towards 280 nm, which was observed at low concentrations (see figure 1), the Ce^{3+} emission of the CsY_2F_7 : 0.12 mol% Ce^{3+} sample overlaps the absorption band at 295 nm. This absorption band is therefore not correctly measured since the light emitted by the sample upon illumination with UV photons partially cancels the loss of photons due to absorption in this region.

3.3. Photon excitation data

In order to obtain more insight into the physical processes that lead to the gamma-induced emission characteristics described above, VUV excitation measurements were performed.

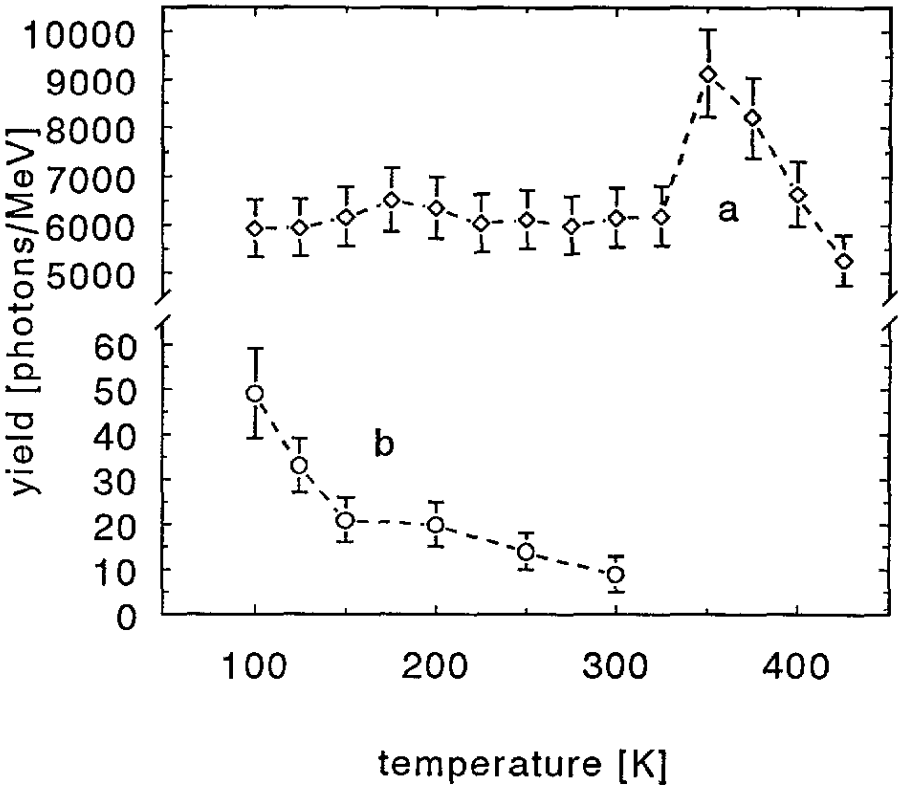

Figure 5. The integral light yield as a function of temperature of the Ce^{3+} luminescence observed in (a) 1.55 mm thick $CsGd_2F_7$: 10 mol% Ce^{3+} (corrected for absorption) and (b) unpolished $CsGd_2F_7$: 0.004 mol% (uncorrected for absorption).

Quantum efficiencies presented in this section are estimations obtained by the procedure described in section 2.

3.3.1. STE luminescence. We will first pay some attention to the long-wavelength emission, as it is observed in both $CsGd_2F_7$ and CsY_2F_7 crystals. As an example, the excitation spectrum of this emission as measured in $CsGd_2F_7$: 0.1 mol% Ce^{3+} is shown in figure 8. In other $CsGd_2F_7$ and CsY_2F_7 crystals similar spectra were measured. The excitation spectrum consists of a single small band at about 167 nm, which is in fact located on the fundamental absorption edge of $CsGd_2F_7$ and CsY_2F_7 (see figure 7). Excitation in this band yields a broad emission band at around 445 nm, also shown in figure 8. As was already mentioned the intensity of this band upon x-ray excitation shows no apparent relation to the Ce^{3+} concentration and increases sharply as the temperature decreases from 300 to 95 K (see figure 3). All the above characteristics are typical for STE luminescence so we identify this emission as such. The fact that the lowest-energy peak of the excitation spectrum is usually located on the STE absorption edge and not at the actual absorption peak wavelength is commonly explained as being caused by the quenching of STE's in a surface layer of the crystal, where most of the incident photons are absorbed at this wavelength [9, 10]. Another factor is the reflection of incident photons which is relatively strong if μ is high. As a result of these phenomena the excitation spectrum of an STE is usually anticorrelated

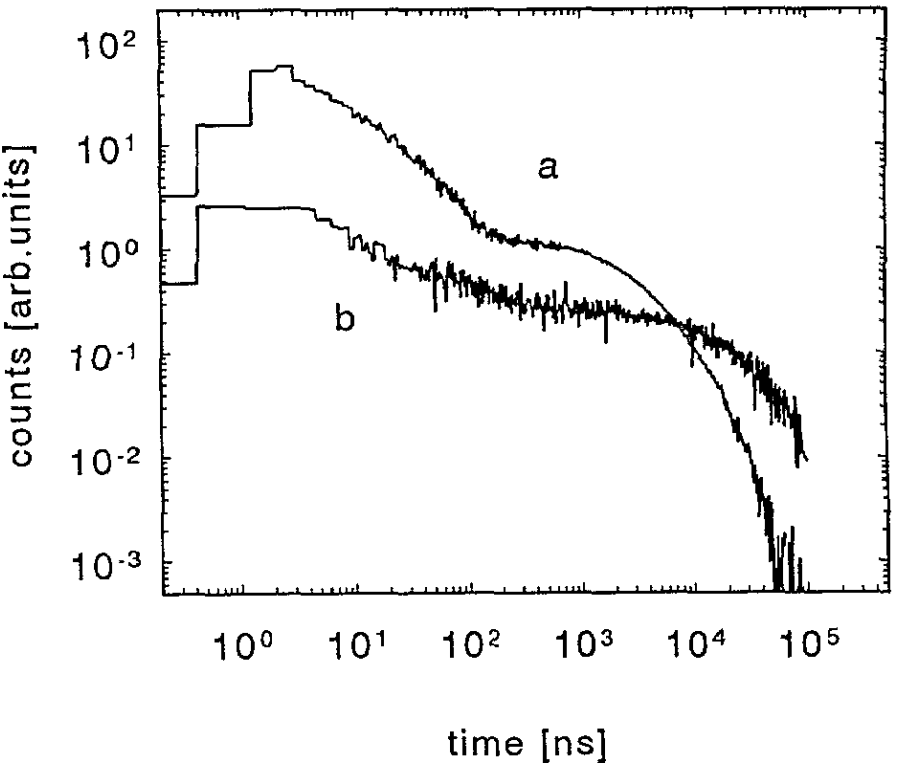

Figure 6. Scintillation decay spectra of (a) $CsGd_2F_7$: 10 mol% Ce^{3+} and (b) $CsGd_2F_7$: 3 mol% Ce^{3+} as measured using the single-photon-counting technique described in section 2.

with the absorption (or reflection) spectrum.

We will now focus on the excitation characteristics of the Ce^{3+} luminescence in CsY_2F_7 and $CsGd_2F_7$, respectively. From the information presented we will eventually derive the energy level scheme shown in figure 13.

3.3.2. $CsY_2F_7:Ce^{3+}$. In figure 9 two emission spectra as measured by exciting a sample of CsY_2F_7 : 0.08 mol% with photons of 295 and 270 nm, being the peak wavelengths of the two lowest-energy Ce^{3+} absorption bands (see figure 7), are presented. It is clear that these bands give rise to different emissions which have a rather similar shape, but are shifted relative to each other. We will denote these emissions as Ce_1^{3+} (maximum at 310 nm) and Ce_2^{3+} (maximum at 333 nm). We have verified that, as was mentioned in section 3.1.1, the x-ray-induced Ce^{3+} emission spectrum of CsY_2F_7 : 0.08 mol% Ce^{3+} can be constructed by adding the Ce_1^{3+} and Ce_2^{3+} emission spectra in the correct ratio. The same holds for the $CsY_2F_7:Ce^{3+}$ samples with other Ce^{3+} concentrations.

To investigate the relationship between the Ce_1^{3+} and Ce_2^{3+} emission bands and the observed Ce^{3+} absorption spectrum, excitation spectra were recorded for emission wavelengths of 295 and 365 nm (see figure 10), chosen such that the Ce_1^{3+} luminescence was monitored with as little interference with the Ce_2^{3+} luminescence as possible, and vice versa.

The excitation spectrum of the Ce_1^{3+} emission band consists of five bands located at about 265, 252, 226, 197 and 188 nm. We will denote these as the Ce_1^{3+} 5d(1) to 5d(5)

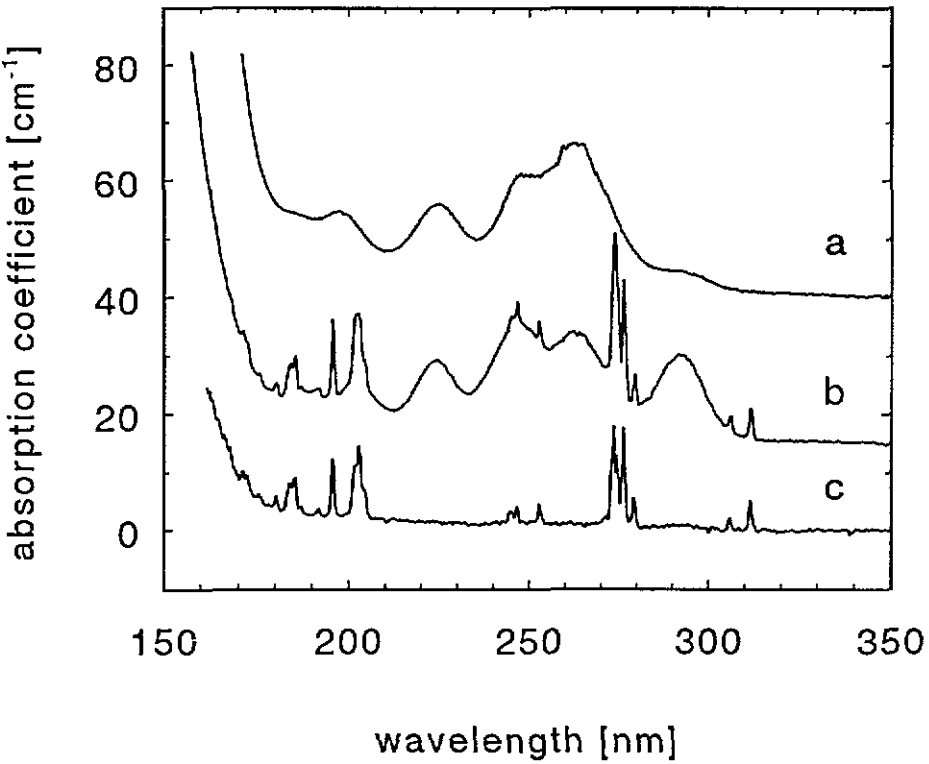

Figure 7. Optical absorption spectra of (a) 1.5 mm thick CsY_2F_7 : 0.12 mol% Ce^{3+}, (b) 1.35 mm thick $CsGd_2F_7$: 0.1 mol% Ce^{3+} and (c) unpolished $CsGd_2F_7$: 0.004 mol%. The wavelength resolution is 0.2 nm. For clarity, spectra (a) and (b) have been shifted by 15 and 40 cm^{-1}, respectively.

absorption bands; see figure 13.

The excitation spectrum of the Ce_2^{3+} emission is a bit more complicated. At least six maxima are visible, at roughly the same wavelengths as the Ce^{3+} absorption peaks in figure 7. In order to understand this spectrum we observe that the Ce_1^{3+} emission (figure 9) overlaps the Ce_2^{3+} absorption band at 295 nm. This makes $Ce_1^{3+} \rightarrow Ce_2^{3+}$ energy transfer very likely to occur. Consequently, excitation of the Ce_1^{3+} centres should result in an emission spectrum which is composed of both the Ce_1^{3+} and Ce_2^{3+} emission bands. This is indeed the case for the emission spectrum upon excitation in the Ce_1^{3+} 5d(1) band ($\lambda_{ex} = 270$ nm); see the dashed curve in figure 9. One also expects to see a contribution of the excitation spectrum of the Ce_1^{3+} emission in the excitation spectrum of the Ce_2^{3+} emission. Indeed, when a proper amount of the first (i.e. the dashed) curve in figure 10, is subtracted from the latter, one is left with a spectrum consisting of five bands at about 295, 237, 221, 202 and 186 nm (see also figure 12), which we will denote as the Ce_2^{3+} 5d(1) to 5d(5) absorption bands; see figure 13. The resulting spectrum is zero around 270 nm, where only the Ce_1^{3+} 5d(1) band is located. This implies that, for $\lambda_{ex} = 270$ nm, the Ce_2^{3+} emission is only excited indirectly via $Ce_1^{3+} \rightarrow Ce_2^{3+}$ transfer.

It is now not hard to see that the Ce^{3+} absorption spectrum of $CsY_2F_7:Ce^{3+}$ shown in figure 7 is actually composed of the Ce_1^{3+} and Ce_2^{3+} absorption bands. We think of these as the fivefold-splitted 5d absorption levels of two different types of Ce^{3+} centre, presumably

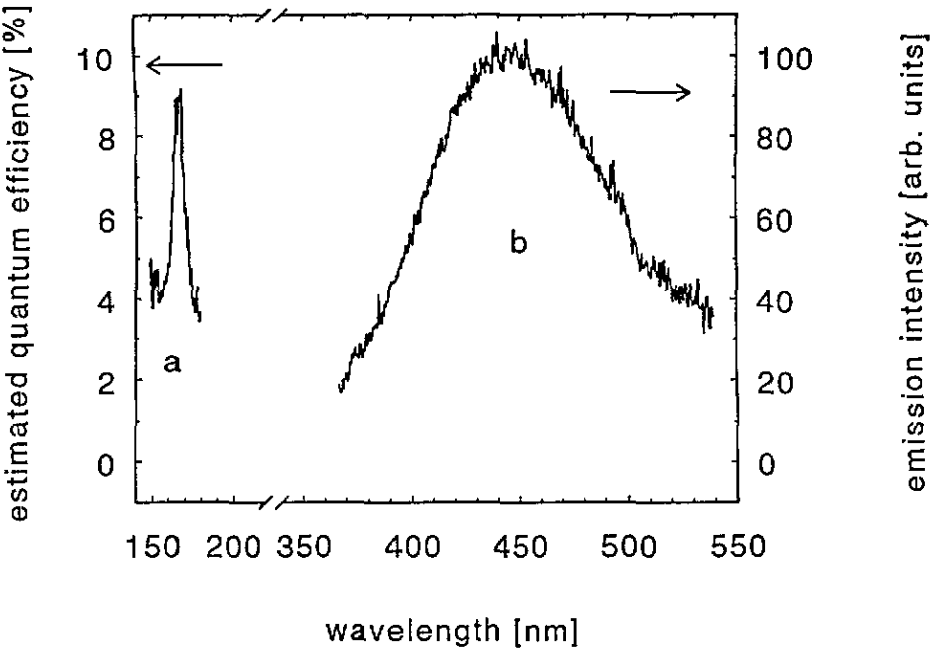

Figure 8. The excitation spectrum (a) for λ_{em} = 440 nm and emission spectrum (b) for λ_{ex} = 160 nm of the STE emission observed in $CsGd_2F_7$: 0.1 mol% at 93 K. The resolutions are (a) 4 nm and (b) 16 nm.

Ce^{3+} ions at different crystallographic sites, which we already denoted as Ce_1^{3+} (310 nm emission) and Ce_2^{3+} (333 nm emission) centres.

In figure 11 the decay spectrum of the Ce_2^{3+} luminescence upon excitation with 290 nm photons is shown as curve a. This curve can be described quite well by a single exponential with $\tau = 32$ ns. Although the decay curve of the Ce_1^{3+} centres was not measured, one may expect the intrinsic decay constant of these centres to be about 26 ns, assuming that $\tau \sim \nu^{-3}$, where ν is the emission wave number [20].

Using the information presented above we will try to account for the scintillation properties of CsY_2F_7. The fact that the Ce^{3+} excitation spectrum of CsY_2F_7 : 0.08 mol% Ce^{3+} was found to be zero between 30 and 170 nm indicates that there is no efficient energy transfer from the host lattice to the Ce^{3+} ions. In other words the electron–hole pairs created upon gamma irradiation do not excite the Ce^{3+} ions efficiently. A possible explanation can be that the probability for these to form STEs is much higher. From the excitation and absorption data it follows that STE $\rightarrow$ Ce^{3+} transfer is not possible since the Ce^{3+} absorption bands are at shorter wavelengths than the STE emission. We therefore suggest that the Ce^{3+} ions are only excited directly in the ionization track of the primary hot electrons created upon absorption of a gamma quantum. This is consistent with the low photon yield.

We showed that $Ce_1^{3+} \rightarrow Ce_2^{3+}$ energy transfer takes place in the 0.08 mol% doped CsY_2F_7 sample. In view of the low Ce^{3+} concentration, this may be largely due to radiative transfer, i.e. absorption by Ce_2^{3+} of photons emitted by Ce_1^{3+} centres. For large Ce^{3+} concentrations $Ce_1^{3+} \rightarrow Ce_2^{3+}$ transfer by non-radiative processes may be dominating. Since these processes can be much faster than the Ce_1^{3+} radiative decay, one then expects a quenching of the Ce_1^{3+} emission with increasing Ce^{3+} concentration. This is indeed observed

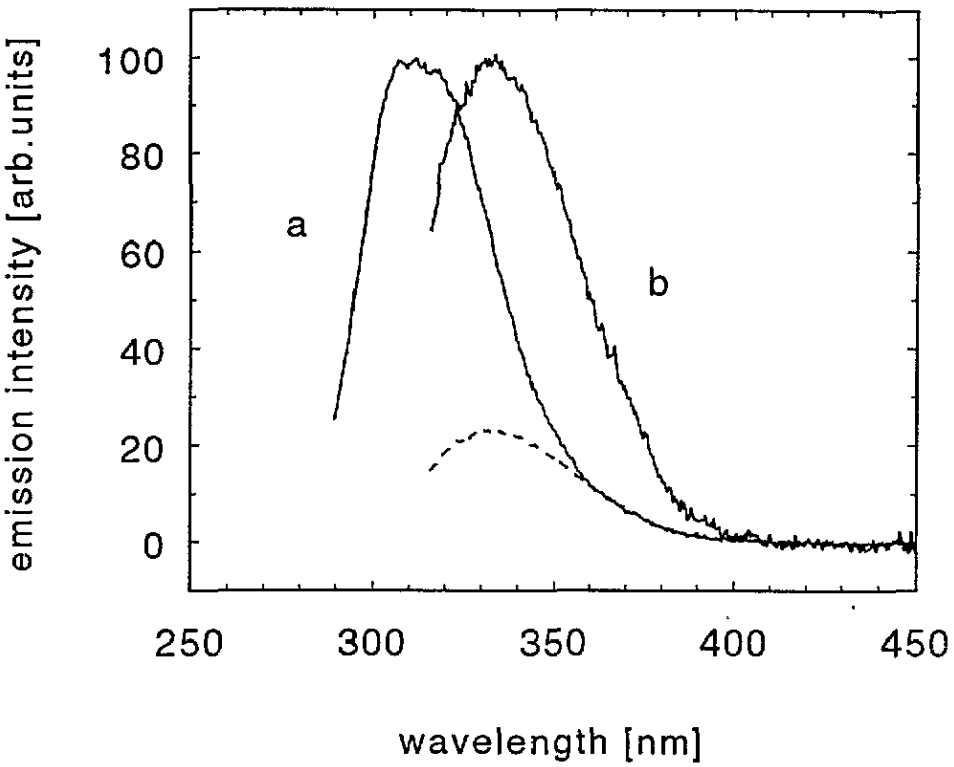

Figure 9. UV-excited emission spectra of CsY_2F_7 : 0.08 mol% Ce^{3+} for (a) λ_{ex} = 270 nm and (b) λ_{ex} = 295 nm at room temperature. The maxima of both spectra were normalized to 100. The dashed line indicates the amount of Ce_2^{3+} luminescence in spectrum (a); see the text for further explanation. The resolution is 16 nm.

in the x-ray emission spectra of $CsY_2F_7:Ce^{3+}$; see figure 1.

Recently we reported on a somewhat similar case [11, 12, 13]. In these works a detailed study of different Ce^{3+} centres found in BaF_2:Ce and the processes through which energy transfer occurs between these centres was presented. The existence of multiple types of Ce^{3+} centre has been reported in other systems as well [14, 15, 16, 17], which seems to indicate that it is not at all a rare phenomenon.

In figure 11 the 662 keV excited scintillation decay spectrum of CsY_2F_7 : 5 mol% Ce^{3+} is shown as curve b. This curve is quite similar to the photon-excited Ce_2^{3+} decay spectrum shown as curve a, which is easily explained if the above suggestions are true. In that case one expects the scintillation decay spectrum to be composed of two components. The first originates from directly excited Ce_2^{3+} ions, yielding a single exponential with a decay time of 32 ns. The second originates from Ce_2^{3+} ions indirectly excited via non-radiative $Ce_1^{3+} \rightarrow Ce_2^{3+}$ transfer. If this transfer is indeed much faster than the Ce_2^{3+} radiative decay the latter will determine the effective decay time, which will thus approximately be 32 ns, too. The small fast component visible in the first 5 ns of the scintillation decay spectrum (curve b) is ascribed to a small remainder of Ce_1^{3+} luminescence which is strongly quenched due to $Ce_1^{3+} \rightarrow Ce_2^{3+}$ transfer.

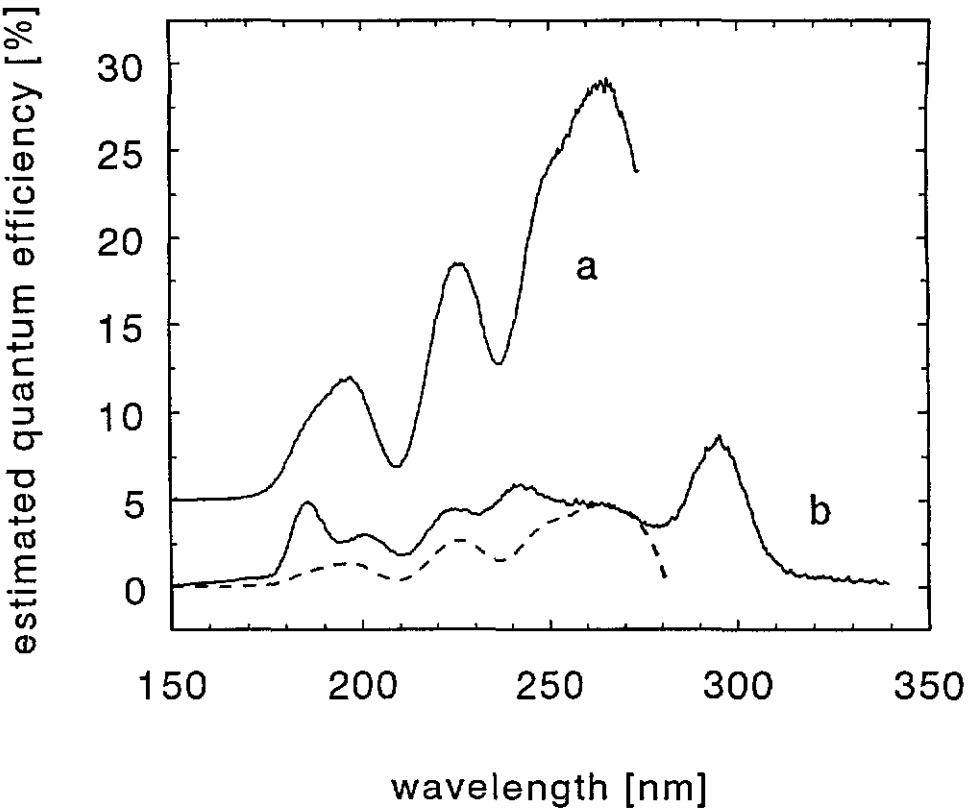

Figure 10. Excitation spectra of $CsY_2F_7 : 0.08\ Ce^{3+}$ for (a) $\lambda_{em} = 295$ nm and (b) $\lambda_{em} = 365$ nm at room temperature. For clarity, spectrum (a) is shifted by 5%. The dashed line indicates the part of spectrum (b) which originates from $Ce_1^{3+} \rightarrow Ce_2^{3+}$ transfer (see the text). The resolution is 8 nm.

3.3.3. $CsGd_2F_7 : Ce^{3+}$. Since the $CsGd_2F_7$ and CsY_2F_7 crystal structures are equal, one expects the same two Ce^{3+} centres as were found in CsY_2F_7 to be present in $CsGd_2F_7$. This is confirmed by the fact that the Ce^{3+} absorption spectra are similar. Furthermore the x-ray emission spectra of both CsY_2F_7 and $CsGd_2F_7$ doped with a few mol% of Ce^{3+} or more can be described as consisting of only a Ce_2^{3+} emission band; see figures 4 and 9. However, while samples of CsY_2F_7 with lower Ce^{3+} concentrations show a contribution of Ce_1^{3+} luminescence, this is not observed in any of the $CsGd_2F_7 : Ce^{3+}$ samples.

In order to find an explanation for this difference, we consider the possible consequences of the presence of Gd^{3+} as a constituent of the host lattice in $CsGd_2F_7$. A number of compounds are known in which energy migration over the Gd^{3+} sublattice is very effective since the non-radiative energy transfer probability $\Gamma_{Gd \rightarrow Gd}$ between neighbouring Gd^{3+} ions is many orders of magnitude higher than the Gd^{3+} radiative decay rate Γ_{Gd}^{rad}; see for example, [6, 18, 19] or [20] and references therein. If transfer over the Gd^{3+} sublattice to other optically active centres is possible, this often has a dominating influence on the luminescence properties of the material.

According to the Förster–Dexter model, energy transfer between optical centres is possible if two conditions are fulfilled [21]. Firstly some interaction mechanism between the centres (multipole–multipole or exchange) must exist and secondly the emission spectrum

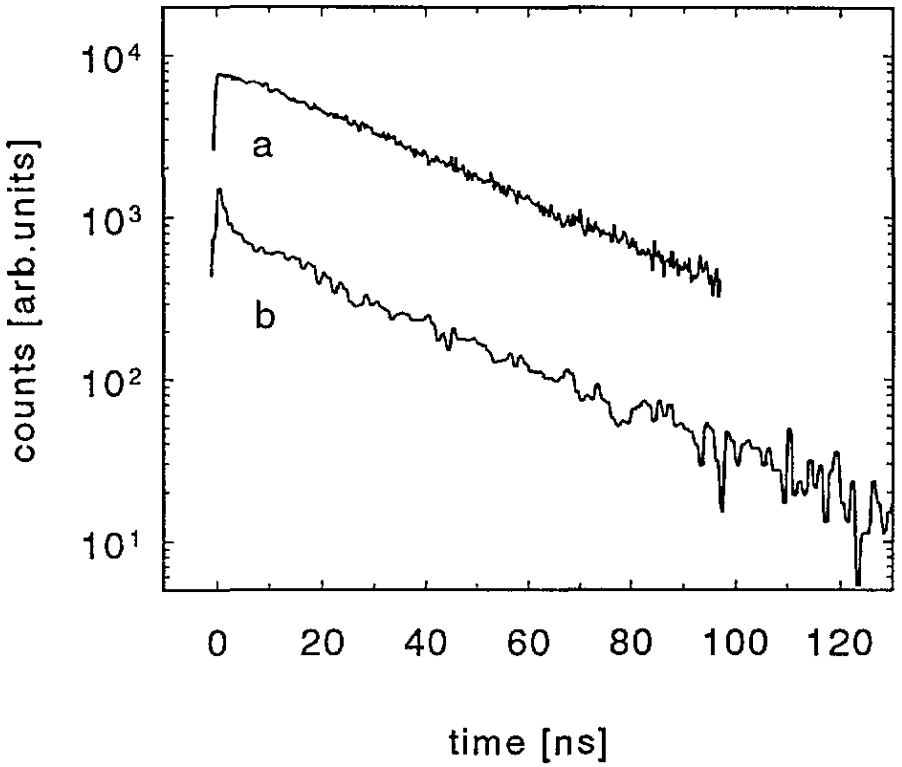

Figure 11. The UV-induced decay spectrum (a) of $CsY_2F_7:0.08$ mol% Ce^{3+} at λ_{ex} = 290 nm and λ_{em} = 340 nm and scintillation decay curve (b) of $CsY_2F_7:5$ mol% Ce^{3+}. The spectra were measured at room temperature.

of the donor centre must show some spectral overlap with the absorption spectrum of the acceptor. The transfer probability is proportional to the overlap integral.

From the absorption spectra presented in figure 7 we observe that the Ce_1^{3+} emission shown in figure 9 overlaps the Gd^{3+} ^6P lines of $CsGd_2F_7$, thereby making $Ce_1^{3+} \rightarrow Gd^{3+}$ transfer possible. Since the lowest Gd^{3+} ^6P line overlaps both the Ce_2^{3+} emission and 5d(1) absorption bands, $Ce_2^{3+} \rightarrow Gd^{3+}$ as well as $Gd^{3+} \rightarrow Ce_2^{3+}$ transfer is possible, although the overlap in these cases is smaller than in the case of $Ce_1^{3+} \rightarrow Gd^{3+}$ transfer. In the energy level scheme shown in figure 13 these transfer probabilities are indicated by arrows.

In figure 12 the Ce^{3+} excitation spectrum of $CsGd_2F_7:0.1$ mol% Ce^{3+} at room temperature is shown. Several Gd^{3+} lines are visible, especially the 312 nm line, which clearly proves that $Gd^{3+} \rightarrow Ce_2^{3+}$ transfer does indeed occur.

When the crystal is cooled down to 95 K some interesting changes occur; see figure 12. On lowering the temperature the thermal broadening of the 295 nm Ce_2^{3+} absorption band reduces. As a result the overlap with the 312 nm Gd^{3+} emission line diminishes causing the disappearance of the 312 nm line in the Ce_2^{3+} excitation spectrum. This means that $Gd^{3+} \rightarrow Ce_2^{3+}$ transfer via the Gd^{3+} $^6P_{3/2}$ level becomes much less efficient. We also note that the spectrum is zero around 270 nm, where the Ce_1^{3+} 5d(1) band is located. This and the fact that no Ce_1^{3+} emission is observed leads to the idea that complete $Ce_1^{3+} \rightarrow Gd^{3+}$ transfer occurs. While at room temperature this can be followed by $Gd^{3+} \rightarrow Ce_2^{3+}$ transfer, this is negligible at 95 K. The five bands visible in the excitation spectrum at 95 K

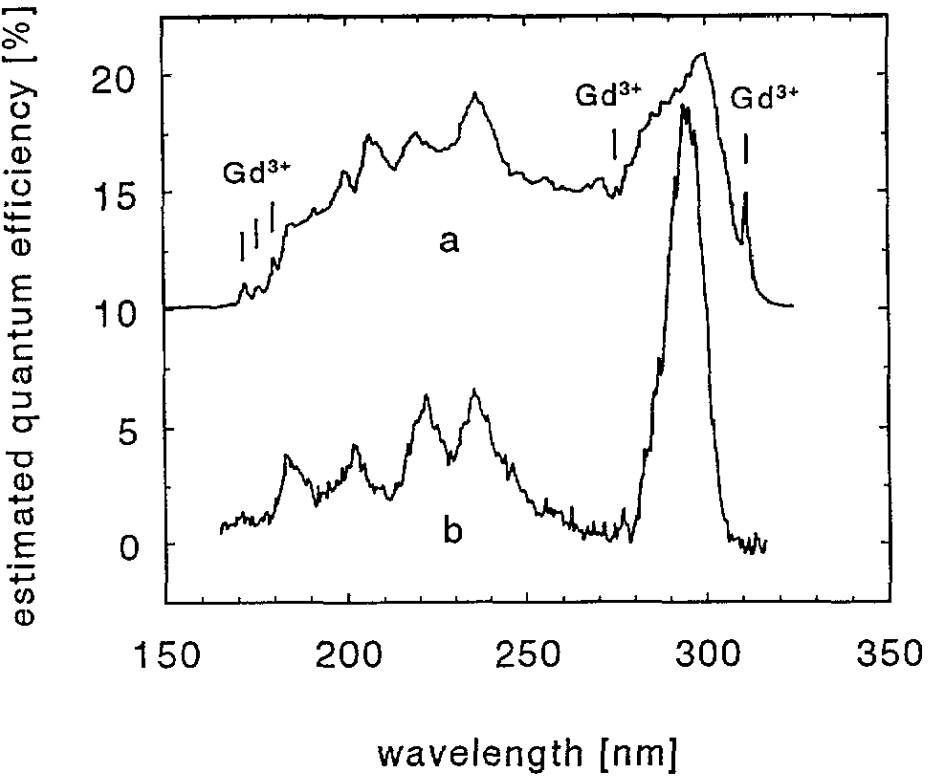

Figure 12. Excitation spectra of $CsGd_2F_7:0.1$ mol% Ce^{3+} for λ_{em} = 340 nm at (a) room temperature and (b) 95 K. For clarity, spectrum (b) is shifted by 10%. The resolutions are (a) 1 nm and (b) 4 nm.

must then be the Ce_2^{3+} 5d levels. These are indeed precisely the same bands as were found when the Ce_2^{3+} excitation spectrum of CsY_2F_7 was corrected for $Ce_1^{3+} \rightarrow Ce_2^{3+}$ transfer; see figure 10. We conclude that the $Ce_1^{3+} \rightarrow Gd^{3+}$ transfer rate between nearest neighbours $\Gamma_{Ce1 \rightarrow Gd}$, multiplied by the number of nearest Gd^{3+} neighbours, is at least about two orders of magnitude larger than the Ce_1^{3+} radiative decay rate Γ_{Ce1}^{rad}, which is about 4×10^7 s^{-1}; see section 3.3.2. This implies $\Gamma_{Ce1 \rightarrow Gd} \geqslant 10^9$ s^{-1}.

The luminescence properties of $CsGd_2F_7:Ce^{3+}$ show many similarities to those of $RbGd_2F_7:Ce^{3+}$ reported in [6]. In $RbGd_2F_7:Ce^{3+}$ two Ce^{3+} absorption bands were measured at 290 and 260 nm. The first transfers its energy partly to Gd^{3+}, the latter completely. The similarity is not unexpected considering that $RbGd_2F_7$ and $CsGd_2F_7$ have equal crystal structures [5]. In [6], the two bands were identified as the 5d(1) and 5d(2) absorption bands of a single type of Ce^{3+} centre. This would imply that this Ce^{3+} centre, when excited to the 5d(2) state, completely transfers its energy to Gd^{3+} instead of relaxing to the 5d(1) state. In view of our results, however, we propose that the 260 and 290 nm bands in $RbGd_2F_7:Ce^{3+}$ are in fact the 5d(1) absorption bands of two different Ce^{3+} centres, similar to the Ce_1^{3+} and Ce_2^{3+} centres in CsY_2F_7 and $CsGd_2F_7$.

So far we have not discussed $Ce_2^{3+} \rightarrow Gd^{3+}$ transfer. The emission spectrum of, e.g., $CsGd_2F_7:0.3$ mol% Ce^{3+} at 300 K upon excitation into the Ce_2^{3+} 5d(1) level (λ_{ex} = 290 nm) shows a 312 nm Gd^{3+} line of about 2.5% of the integral Ce^{3+} luminescence intensity. Taking into account that also $Gd^{3+} \rightarrow Ce_2^{3+}$ backtransfer occurs this means that (possibly much)

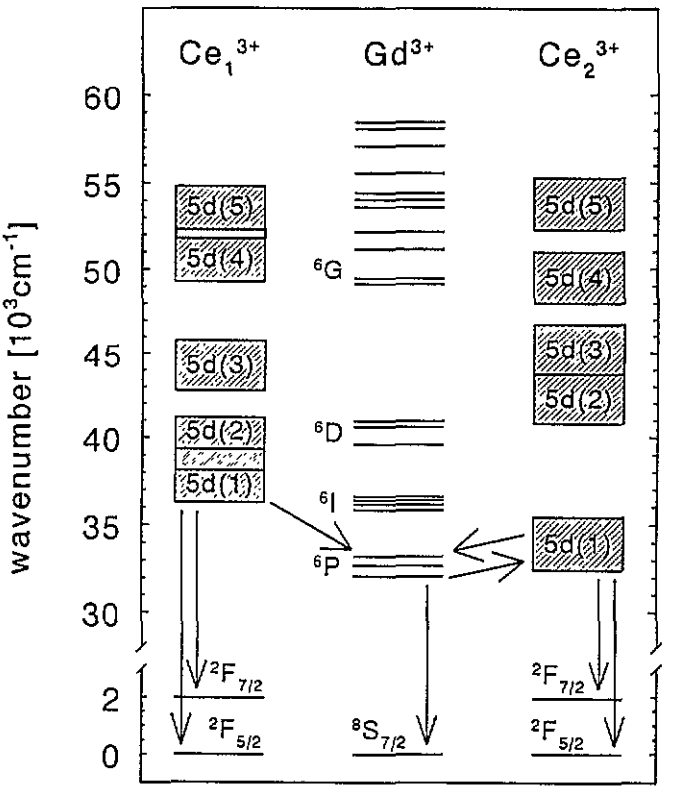

Figure 13. The energy level scheme of Ce_1^{3+}, Ce_2^{3+} and Gd^{3+} centres in $CsY_2F_7:Ce^{3+}$ and $CsGd_2F_7:Ce^{3+}$. The unrelaxed excited 5d states of Ce_1^{3+} and Ce_2^{3+} as determined from excitation measurements are represented as shaded areas, the states of the $4f^7$ configuration of Gd^{3+} as determined from absorption spectra are shown as solid lines. Some important transfer and radiative decay processes are indicated by arrows.

more than 2.5% of the initial energy is transferred to the Gd^{3+} sublattice.

Figure 14 shows the UV-induced decay spectra of $CsGd_2F_7:0.3$ and 10 mol% Ce^{3+}. The decay curves of the Ce_2^{3+} luminescence of $CsGd_2F_7:0.3$ and 10 mol% Ce^{3+} are rather similar, except in the first 10 ns, where the luminescence decay of the 0.3 mol% doped sample is faster. In both cases the decay rate in this region is considerably faster than the decay rate of 32 ns observed in CsY_2F_7, indicating that the Ce_2^{3+} emission in $CsGd_2F_7$ is quenched due to $Ce_2^{3+} \rightarrow Gd^{3+}$ transfer. We conclude that the $Ce_2^{3+} \rightarrow Gd^{3+}$ transfer rate $\Gamma_{Ce2\rightarrow Gd}$ multiplied by the number of nearest Gd^{3+} neighbours must be of the same order of magnitude as the Ce_2^{3+} radiative decay rate Γ_{Ce2}^{rad}, which equals $3.1 \times 10^7\ s^{-1}$, at all Ce^{3+} concentrations.

Based on the data presented above we will now suggest a qualitative model of the scintillation mechanism of $CsGd_2F_7:Ce^{3+}$. In the x-ray-excited emission spectra of $CsGd_2F_7:0.004$ mol% Ce^{3+} between 95 K and room temperature, Gd^{3+} ^6G, ^6D and ^6I lines are visible; see figure 4. This implies that the transition rates from these levels to lower excited $4f^7$ levels are of the same order of magnitude as their radiative decay rates to the ground state, which are of the order of 10^3 to $10^2\ s^{-1}$. Therefore, energy migration is just as likely to occur at these levels as it is at the ^6P level. Since each of these levels overlap the Ce^{3+} absorption spectrum, $Gd^{3+} \rightarrow Ce^{3+}$ transfer is also possible from these

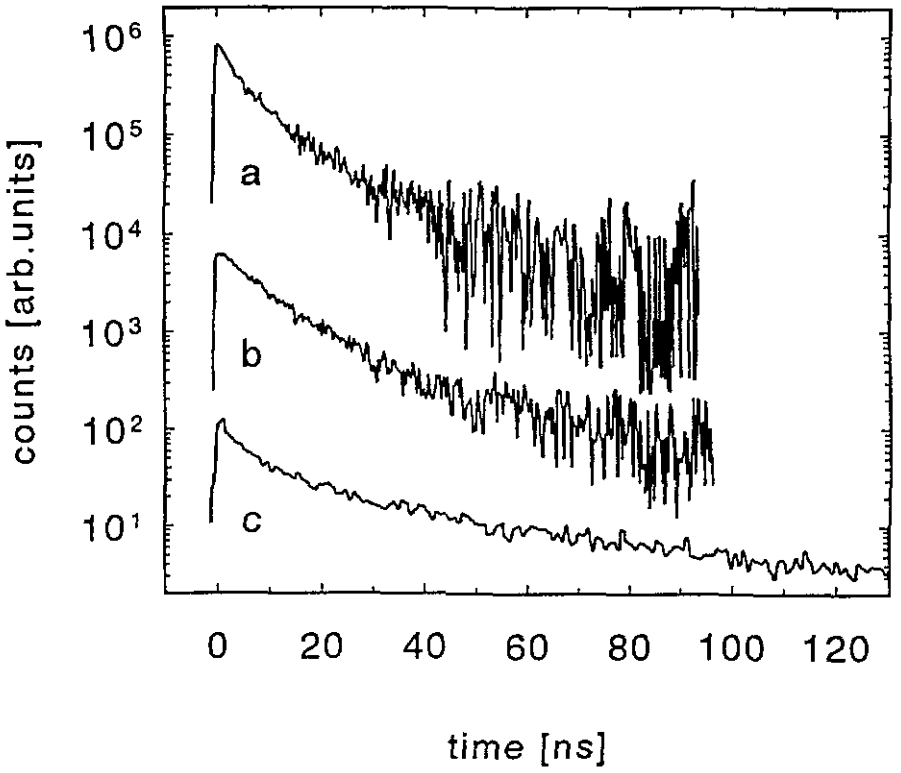

Figure 14. *UV-induced decay spectra at room temperature for excitation in the Ce_2^{3+} 5d(1) level* of (a) $CsGd_2F_7$: 0.3 mol% Ce^{3+} (λ_{ex} = 295, λ_{em} = 340 nm) and (b) $CsGd_2F_7$: 10 mol% Ce^{3+} (λ_{ex} = 300, λ_{em} = 340 nm). Curve (c) is a redraw of the first 130 ns of the scintillation decay curve of $CsGd_2F_7$: 10 mol% Ce^{3+} shown in figure 6.

higher levels.

Consider the situation after absorption of a gamma quantum in which many Ce^{3+} and Gd^{3+} ions, excited to all available energy levels, are present. We envisage the following processes (see also figure 13).

(a) The excited Ce_1^{3+} ions will relax very fast to the 5d(1) level, whereafter all their energy is transferred to the Gd^{3+} ^6P level. At high Ce^{3+} concentrations $Ce_1^{3+} \rightarrow Ce_2^{3+}$ may become important. We will neglect this possibility as it will not have much influence on our conclusions.

(b) The excited Ce_2^{3+} ions will relax too, whereafter some of them transfer their energy to the Gd^{3+} ^6P level, and some decay radiatively with decay characteristics as shown in figure 14.

(c) Gd^{3+} ions excited to the ^6G, ^6D or ^6I levels can (i) relax non-radiatively to lower $4f^7$ levels, (ii) decay radiatively or (iii) transfer their energy to Ce_1^{3+} or Ce_2^{3+} ions, which will be followed by one of the processes described in (a) and (b).

(d) In addition to the population present at the start, the Gd^{3+} ^6P level will be populated via processes (a), (b) and (c). This excitation energy can be emitted as 312 nm photons or transferred to Ce_2^{3+} ions. As was shown, the former possibility occurs only at low Ce^{3+} concentrations.

(e) Instead of energy transport to Ce^{3+} ions, transport to quenching centres may also

occur, which can be a quite efficient process. This process is also known as concentration quenching [20].

In figure 7 one observes that the spectral overlap between the higher Gd^{3+} levels and the Ce^{3+} absorption spectrum is larger than for the ^6P level. Furthermore, $Ce^{3+} \rightarrow Gd^{3+}$ backtransfer to the higher Gd^{3+} levels can be neglected since the non-radiative decay rates of the higher Ce^{3+} 5d levels to lower 5d levels are assumed to be very high. Consequently, $Gd^{3+} \rightarrow Ce^{3+}$ transfer is expected to be much more efficient at the high Gd^{3+} levels than at the ^6P level and will thus be the most probable of the processes mentioned under (c), except at very low Ce^{3+} concentrations. As a result the effective decay rate of the high Gd^{3+} levels should be much larger than that of the ^6P level. This, plus the fact that both $\Gamma_{Ce1 \rightarrow Gd}$ and $\Gamma_{Ce2 \rightarrow Gd}$ are large, implies that the initial population of the ^6P level via the processes described in (d) will be faster than its decay. As a result the decay characteristics of the luminescence of Ce_2^{3+} ions excited via the Gd^{3+} ^6P level are mainly determined by the effective decay rate of the Gd^{3+} ^6P level.

With the above we can account for the occurrence of two major components in the gamma-excited decay spectra of $CsGd_2F_7 : Ce^{3+}$. The fast component of the gamma-excited decay spectrum of $CsGd_2F_7$: 10 mol% Ce^{3+} is shown in figure 14 as curve c. Especially in the first 10 ns the spectrum is very similar to curve b. The small peak at $t = 0$ is attributed to Cherenkov luminescence caused by fast electrons created by the 662 keV gamma quanta. We therefore suggest that this component is at least partly due to directly excited Ce_2^{3+} luminescence. This is in agreement with the fact that the intensity of this component in $CsGd_2F_7 : Ce^{3+}$ is much lower than in CsY_2F_7 with comparable Ce^{3+} concentration.

The slow component of the scintillation curve is ascribed to Ce_2^{3+} ions excited via the Gd^{3+} ^6P level. We have argued that the decay time of this component, i.e. τ_s in table 1, is mainly determined by the effective decay rate of the Gd^{3+} ^6P level, although the ^6P level itself is populated via various processes, which may partly explain the non-exponentiality of the slow component. Based on this assumption, in section 4 we will develop a simplified theoretical model which predicts τ_s and the Ce_2^{3+} light yield as a function of Ce^{3+} concentration.

We will now pay some attention to the excitation spectra of $CsGd_2F_7$: 10 mol% Ce^{3+}; see figure 15. At room temperature the individual excitation bands between 200 and 300 nm are indistinguishable. This means that in this region the photons entering the crystal are efficiently absorbed by the Ce^{3+} ions, so the maximum (external) quantum efficiency, which is then only limited by reflective losses and quenching, is reached at all wavelengths. Since at this concentration the optical absorption coefficient of Ce^{3+} is much higher than that of Gd^{3+}, virtually no Gd^{3+} ions are excited directly by the incident photons, and thus no Gd^{3+} lines are visible in the spectrum.

The spectrum at 95 K is actually quite surprising. It appears to be anticorrelated to the Ce^{3+} absorption spectrum as measured for $CsGd_2F_7$: 0.1 mol% Ce^{3+}; see figure 7. This anticorrelation is usually found in the case of STE luminescence, and has been explained as a surface effect. However, the absorption strength of Ce^{3+} ions is much less than that of STEs. If we assume the absorption spectrum of $CsGd_2F_7$: 10 mol% Ce^{3+} to be equal to that of $CsGd_2F_7$: 0.1 mol% Ce^{3+} times 10^2, at $\lambda = 245$ nm half of the photons are absorbed in a layer of thickness $d_{1/2} \equiv \ln(2)/\mu \approx 3$ μm, so we can hardly claim that the photons are absorbed in a surface layer. We should, however, consider the fact that a major part of the excitation energy on the Ce^{3+} ions is transferred to the Gd^{3+} ^6P level, whereafter the energy quanta migrate over the Gd^{3+} sublattice during a mean time t, which is equal to the effective decay rate of the Gd^{3+} ^6P level. We therefore propose the existence of an

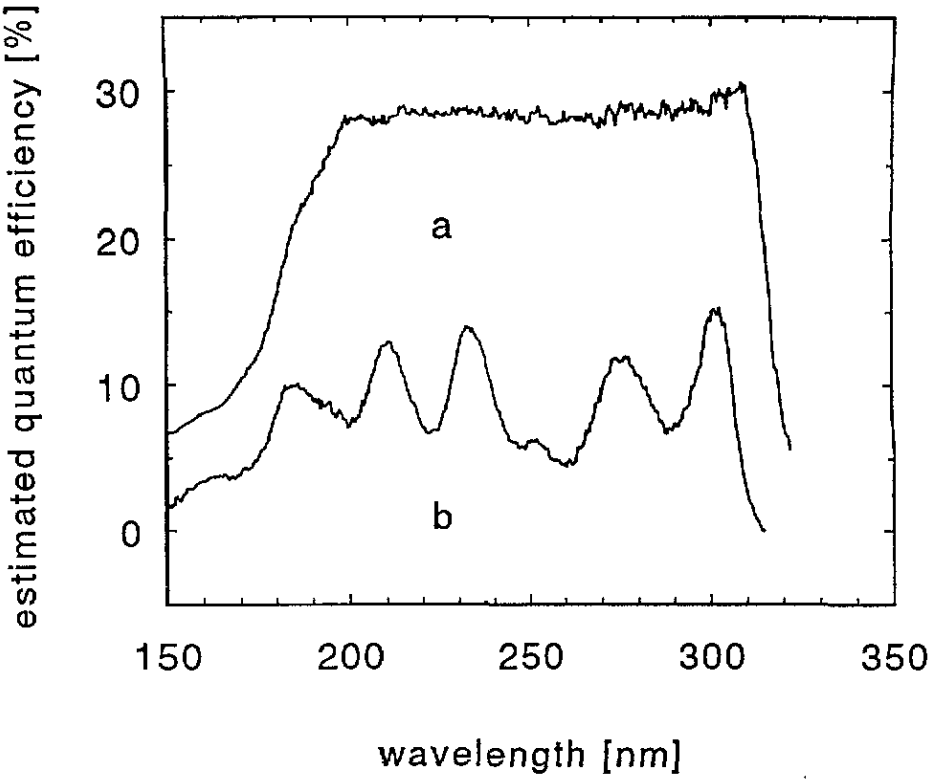

Figure 15. Excitation spectra of $CsGd_2F_7$: 10 mol% Ce^{3+} for λ_{em} = 340 nm at (a) room temperature and (b) 95 K. For clarity, spectrum (a) is shifted by 5%. The resolution is 4 nm.

'extended surface layer' having a thickness equal to the mean displacement of the excitation quanta, in which a substantial part of the absorbed excitation energy is transported to the actual crystal surface where it is lost by non-radiative recombination processes. Of course this effect will be strongest at wavelengths at which μ is high, which may explain the anticorrelation between the excitation and absorption spectra.

As an order-of-magnitude approximation for the thickness of this layer we will assume that the migration of an excitation quantum over the Gd^{3+} sublattice can be described as a three-dimensional random walk during a length of time equal to t. The root mean square displacement of a large number of excitations can then be approximated using:

$$\sqrt{\langle r^2(t)\rangle} \approx \ell^2 \Gamma_j t$$

where Γ_j is the mean jump rate and ℓ the mean length of a jump.

Let us first consider the situation in the 10 mol% doped sample at 95 K. If we assume in first instance that $\Gamma_{Gd\rightarrow Ce2} = 0$ at this temperature and if we neglect transfer to quenching centres, then the effective decay rate of the Gd^{3+} ^6P level must be equal to Γ_{Gd}^{rad}. With ℓ = 0.4 nm, $\Gamma_j = \Gamma_{Gd\rightarrow Gd} = 10^9$ s^{-1} and $t = (\Gamma_{Gd}^{rad})^{-1} = 10^{-2}$ s, which are realistic values [20], we find $\sqrt{\langle r^2\rangle} \approx 1.3$ μm. We observe that the estimations of $d_{1/2}$ and $\sqrt{\langle r^2\rangle}$ are of the same order of magnitude at this temperature, which supports the above suggestion.

At room temperature we can estimate $\sqrt{\langle r^2\rangle}$ using $t = \tau_s = 7$ μs; see table 1. This gives a value of 33 nm, which is much smaller than $d_{1/2}$, so at room temperature one does not expect there to be much of an effect on the excitation spectrum, as is indeed found to

be the case.

At low Ce^{3+} concentrations this effect does not occur at all since the mean migration time t is limited to $(\Gamma_{Gd}^{rad})^{-1}$, so the maximum thickness of the 'extended surface layer' is 1.3 μm as was calculated above. At 0.1 mol% Ce^{3+} we find $d_{1/2} \approx 0.3$ mm at 245 nm, which is much larger.

This 'extended surface layer' effect is an interesting consequence of the occurrence of energy migration which has as far as we know not been reported on before.

4. Model calculations and discussion

In this section we develop a simple theoretical model for the scintillation properties of $CsGd_2F_7:Ce^{3+}$, which accounts for the presence of a fast decay component and a slow one. In section 3.3.3 we argued that the effective decay rate of the Gd^{3+} ^6P level, which we will hereafter denote as Γ_s, determines the decay rate of the dominating slow component, while the decay rate of the fast component is determined by the decay rate of directly excited Ce_2^{3+} ions, which we will denote as Γ_f. In the following we neglect the initial relaxation processes mentioned under (a), (b) and (c) in section 3.3.3. Furthermore, as $Ce_1^{3+} \rightarrow Gd^{3+}$ transfer is very fast (see section 3.3.3) we will assume that excitation energy present on Ce_1^{3+} ions is instantaneously transferred to the Gd^{3+} sublattice whereafter the Ce_1^{3+} ions can be considered as inert lattice constituents. We thus start from a situation after absorption of a gamma quantum, in which a number of $N(0)$ excitation quanta are present in the lattice, of which $N_{Ce2}(0)$ and $N_{Gd}(0)$ reside on the Ce_2^{3+} 5d(1) and Gd^{3+} ^6P levels, respectively; see figure 13. Direct energy transfer from Ce_2^{3+} ions to quenching centres is neglected, but transport of energy to quenching centres over the Gd^{3+} sublattice is accounted for, as it will be of importance at low Ce^{3+} concentrations. We start with the rate equations, in which we deal exclusively with nearest-neighbour interactions:

$$dN_{Ce2}(t) = \{-\Gamma_{Ce2}^{rad} N_{Ce2}(t) + \Gamma_{Gd\rightarrow Ce2}\,\bar{n}_{Ce2}\,N_{Gd}(t) - \Gamma_{Ce2\rightarrow Gd}\,\bar{n}_{Gd}\,N_{Ce2}(t)\}\,dt \quad (1)$$

$$dN_{Gd}(t) = \{-(\Gamma_{Gd}^{rad} + \Gamma_{Gd}^{Q})\,N_{Gd}(t) - \Gamma_{Gd\rightarrow Ce2}\,\bar{n}_{Ce2}\,N_{Gd}(t) + \Gamma_{Ce2\rightarrow Gd}\,\bar{n}_{Gd}\,N_{Ce2}(t)\}\,dt. \quad (2)$$

The first term in equation (1) is the number of radiatively decaying Ce_2^{3+} centres per unit time. In the first term of equation (2) a mean quenching rate Γ_{Gd}^{Q} is added to the Gd^{3+} radiative decay rate Γ_{Gd}^{rad}. This is justified if $Gd^{3+} \rightarrow Gd^{3+}$ energy transfer is so fast that transport to quenching centres is not limited by energy migration, so all excitation quanta on the Gd^{3+} sublattice have the same probability of being transferred to a quenching centre. The second terms of the rate equations (1) and (2) represent transfer of energy from Gd^{3+} centres to neighbouring Ce_2^{3+} ions. In these terms $\bar{n}_{Ce2}$ is the mean number of Ce_2^{3+} ions neighbouring a Gd^{3+} ion. Again, the use of a mean number of nearest neighbours is justified if energy migration is fast compared to the excitation lifetime. The last term of equations (1) and (2) represents $Ce_2^{3+} \rightarrow Gd^{3+}$ transfer. In this term we use a mean number $\bar{n}_{Gd}$ of Gd^{3+} ions neighbouring a Ce_2^{3+} ion and ignore the fact that the actual number of neighbouring Gd^{3+} ions will vary for individual Ce_2^{3+} ions, as the Ce_2^{3+} ions are distributed randomly over the crystal. Both $\bar{n}_{Ce2}$ and $\bar{n}_{Gd}$ will be functions of the Ce^{3+} concentration, which are determined by the crystal structure, the ratio of the Ce_1^{3+} and Ce_2^{3+} concentrations and the way in which potential Ce_1^{3+} and Ce_2^{3+} sites are distributed over the crystal lattice. In the simplest form these functions can be written as:

$$\bar{n}_{Ce2} = \varphi\,[Ce^{3+}]\,\mathcal{N} \quad (3)$$

$$\bar{n}_{Gd} = (1 - [Ce^{3+}])\,\mathcal{N} \quad (4)$$

where $\mathcal{N}$ is the (mean) coordination number of Gd^{3+} ions surrounding a Gd^{3+} ion in pure $CsGd_2F_7$, φ represents the fraction of Ce^{3+} ions which is of the Ce_2^{3+} type and $[Ce^{3+}]$ is the molar fraction of Ce^{3+} ions.

The two coupled differential equations (1) and (2) can be solved exactly to give

$$N_{Ce2}(t) = (N_{Ce2}(0) - \alpha)\exp(-\Gamma_f t) + \alpha\exp(-\Gamma_s t) \tag{5}$$

$$N_{Gd}(t) = (N_{Gd}(0) - \beta)\exp(-\Gamma_s t) + \beta\exp(-\Gamma_f t) \tag{6}$$

where Γ_f and Γ_s are the two solutions of the quadratic equation

$$\Gamma^2 - (a + c)\Gamma + (ac - bd) = 0 \tag{7}$$

chosen such that $\Gamma_f > \Gamma_s$. In that case Γ_f represents a fast decay component and Γ_s a slow one. In equation (7) we have defined

$$a = \Gamma_{Ce2}^{rad} + d \tag{8}$$

$$b = \Gamma_{Gd\to Ce2}\,\overline{n}_{Ce2} \tag{9}$$

$$c = \Gamma_{Gd}^{rad} + \Gamma_{Gd}^{Q} + b \tag{10}$$

$$d = \Gamma_{Ce2\to Gd}\,\overline{n}_{Gd} \tag{11}$$

The constants α and β are given by

$$\alpha = N_{Gd}(0)\frac{b}{\Gamma_f - \Gamma_s} - N_{Ce2}(0)\frac{a - \Gamma_f}{\Gamma_f - \Gamma_s} \tag{12}$$

$$\beta = (N_{Ce2}(0) - \alpha)\frac{a - \Gamma_f}{b} \tag{13}$$

In order to solve equation (7) it is convenient to write

$$\Gamma = p(a - d) + (1 - p)(c - b) = p\,\Gamma_{Ce2}^{rad} + (1 - p)(\Gamma_{Gd}^{rad} + \Gamma_{Gd}^{Q}) \tag{14}$$

which if substituted into equation (7) provides a quadratic expression for p. This expression has two exact solutions p_f and p_s which are related to Γ_f and Γ_s, respectively.

In the $CsGd_2F_7:Ce^{3+}$ crystals investigated in this work $\Gamma_{Ce2}^{rad} \gg (\Gamma_{Gd}^{rad} + \Gamma_{Gd}^{Q})$, as will be shown later. From equation (14) it is easily seen that p_s must then be the smallest of the two solutions for p. If $p_s \ll 1$, this solution can be approximated, using equations (3) and 4, as

$$p_s \approx \frac{\Gamma_{Gd\to Ce2}\,\varphi\,\mathcal{N}\,[Ce^{3+}]}{\Gamma_{Ce2}^{rad} - \Gamma_{Gd}^{rad} - \Gamma_{Gd}^{Q} + \Gamma_{Ce2\to Gd}(1 - [Ce^{3+}])\mathcal{N}}. \tag{15}$$

In this equation we can approximate $(1 - [Ce^{3+}])$ by 1 if the Ce^{3+} concentration is not too high. This means that, in a first approximation, p_s is proportional to $[Ce^{3+}]$. Note that $\Gamma_{Ce2}^{rad} \approx \Gamma_{Ce2\to Gd}(1 - [Ce^{3+}])\mathcal{N}$; see section 3.3.3.

The parameter p_s has a simple physical interpretation. It represents the fraction of the total number $N(t)$ of excitation quanta residing on Ce_2^{3+} centres in the long-time limit, i.e. at times $t \gg (\Gamma_f)^{-1}$, when the decay is determined by Γ_s.

We can calculate the total Ce_2^{3+} light yield contained in the slow component as

$$Y_{Ce2,s} \equiv \int_0^\infty \Gamma_{Ce2}^{rad}\,\alpha\exp(-\Gamma_s t)\,dt = (N_{Gd}(0) + \alpha - \beta)\frac{p_s\Gamma_{Ce2}^{rad}}{\Gamma_s}. \tag{16}$$

If $\Gamma_{Ce2}^{rad} \gg (\Gamma_{Gd}^{rad} + \Gamma_{Gd}^{Q})$ and $\Gamma_f \gg \Gamma_s$, which is true for the crystals investigated, it can be shown that $\alpha - \beta \approx N_{Ce2}(0)$. We can therefore approximate equation (16) by

$$Y_{Ce2,s} \approx (N_{Gd}(0) + N_{Ce2}(0))\frac{p_s\Gamma_{Ce2}^{rad}}{\Gamma_s} = N(0)\frac{p_s\Gamma_{Ce2}^{rad}}{\Gamma_s}. \tag{17}$$

The ratio of the total light yields of the slow Gd^{3+} and Ce_2^{3+} components equals the ratio of the Gd^{3+} and Ce_2^{3+} luminescence intensities for $t \gg (\Gamma_f)^{-1}$:

$$\frac{Y_{Gd,s}}{Y_{Ce2,s}} = \frac{I_{Gd}(t)}{I_{Ce2}(t)} = \frac{N_{Gd}(t)\,\Gamma_{Gd}^{rad}}{N_{Ce2}(t)\,\Gamma_{Ce2}^{rad}} = \frac{1-p_s}{p_s}\,\frac{\Gamma_{Gd}^{rad}}{\Gamma_{Ce2}^{rad}}. \tag{18}$$

In section 3.3.3 we showed that in $CsGd_2F_7$: 0.3 mol% Ce^{3+} this ratio is about 2.5% for excitation in the Ce_2^{3+} 5d(1) band. With $\Gamma_{Ce2}^{rad} = 3.1 \times 10^7\ s^{-1}$ and $\Gamma_{Gd}^{rad} \approx 10^2\ s^{-1}$ [6], this implies $p_s \approx 0.04[Ce^{3+}]$. We note that equation (15) is a very good approximation for this value of p_s.

Both Γ_f and Γ_s are solutions of equation (7). Consequently, once Γ_s is known, Γ_f can straightforwardly be obtained from

$$\Gamma_f = a + c - \Gamma_s. \tag{19}$$

In the $CsGd_2F_7$: Ce^{3+} crystals investigated Γ_f is many orders of magnitude higher than Γ_s; see the results in table 1. With this and $\Gamma_{Ce2}^{rad} \gg (\Gamma_{Gd}^{rad} + \Gamma_{Gd}^{Q})$ we can approximate equation (19) by

$$\Gamma_f \approx \Gamma_{Ce2}^{rad} + \Gamma_{Ce2\to Gd}\,(1 - [Ce^{3+}])\,\mathcal{N} + \Gamma_{Gd\to Ce2}\,\varphi\,[Ce^{3+}]\,\mathcal{N}. \tag{20}$$

This means that the fast Ce_2^{3+} decay is quenched by energy migration to Gd^{3+}, a conclusion that was already arrived at in section 3.3.3.

We will now evaluate the predictions of the theory presented above on the scintillation properties of the dominating slow component, which where described in section 3.1.2. Equation (15) shows that p_s is in first approximation proportionally to $[Ce^{3+}]$ and becomes very small as $[Ce^{3+}]$ approaches zero. From equation (14) it then follows that at low Ce^{3+} concentrations Γ_s is approximately constant and equal to $(\Gamma_{Gd}^{rad} + \Gamma_{Gd}^{Q})$. In that case equation (17) predicts that $Y_{Ce2,s}$ grows proportionally to $[Ce^{3+}]$. This can be observed in table 1 for $4 \times 10^{-5} < [Ce^{3+}] < 10^{-2}$. For increasing $[Ce^{3+}]$ it appears that $\Gamma_s \approx p_s\Gamma_{Ce2}^{rad}$ and thus increases proportional to $[Ce^{3+}]$. This occurs for $0.03 < [Ce^{3+}] < 0.3$, where τ_s decreases linearly from 22 to 2 μs; see table 1. At the same time equation (17) predicts that the $Y_{Ce2,s}$ approaches $N(0)$. This saturation is indeed observed in table 1. We conclude that $N(0) \approx 6 \times 10^3$ photons MeV^{-1}.

Table 2. Calculated values of τ_s and $Y_{Ce2,s}$ as a function of $[Ce^{3+}]$, obtained with $N(0) = 6\times10^3$ photons MeV^{-1}, $p = 0.038[Ce^{3+}]$, $\Gamma_{Ce2}^{rad} = 3.1 \times 10^7\ s^{-1}$, $(\Gamma_{Gd}^{Q} + \Gamma_{Gd}^{rad}) = 2.3 \times 10^4\ s^{-1}$. The experimental values of the decay rate τ_s and the integral light yield $Y_{Ce2,s}$ of the slow decay component of $CsGd_2F_7$: Ce^{3+} as derived from table 1 are shown for comparison.

Ce concentration (mol%)	τ_s^{calc} (μs)	τ_s^{exp} (μs)	$Y_{Ce2,s}^{calc}$ (photons MeV^{-1})	$Y_{Ce2,s}^{exp}$ (photons MeV^{-1})
30	2.6	2 ± 1	5600	
20	3.8	3 ± 1	5500	5700 ± 700
10	7.1	7 ± 4	5000	5400 ± 600
3	17	22 ± 10	3600	2900 ± 600
1	29		2000	2000 ± 300
0.3	38		800	900 ± 300
0.1	41		290	290 ± 100
0.004	43		12	9 ± 4

In table 2 calculated values of τ_s and $Y_{Ce2,s}$ are listed as a function of $[Ce^{3+}]$. Note that the values of the parameters $N(0)$, p and $(\Gamma_{Gd}^{rad} + \Gamma_{Gd}^{Q})$ used are either very close or

equal to the estimations given above. The value of Γ^{rad}_{Ce2} was derived in section 3.3.2. With $(\Gamma^{rad}_{Gd} + \Gamma^{Q}_{Gd}) = 2.3 \times 10^4$, the calculated values agree very well with the experimental values shown in table 1. The fact that both photon excitation and scintillation data are *predicted* correctly by the above theory using the same set of values for the three free parameters seems a strong confirmation of the correctness of the model of the scintillation mechanism of $CsGd_2F_7 : Ce^{3+}$ developed in this work.

The model allows us to understand other scintillation properties as well. The total Ce^{3+} photon yield of $CsGd_2F_7 : Ce^{3+}$ is much higher than that of CsY_2F_7 with the same Ce^{3+} concentration. This is easily understood if the Ce^{3+} ions in CsY_2F_7 are indeed only excited directly. In $CsGd_2F_7$ the Ce^{3+} ions are additionally excited via the Gd^{3+} sublattice. Apparently a substantial amount of energy is present on this sublattice after absorption of a gamma quantum. We do not know whether this is due to direct Gd^{3+} excitation or (also) to other processes, like relaxation of electrons and holes in the conduction and valence band to the Gd^{3+} ions.

At low Ce^{3+} concentrations the Ce^{3+} intensity was found to increase with decreasing temperature; see figure 5. This may be unexpected as we showed in section 3.3.3 that $\Gamma_{Gd \rightarrow Ce2}$ reduces at low temperatures, which lowers the value of p_s according to equation (15), and thus decreases the value of $Y_{Ce2,s}$; see equation (17). However, $\Gamma_{Ce2 \rightarrow Gd}$ will also decrease which at least partly compensates the decrease of $\Gamma_{Gd \rightarrow Ce2}$ in equation (15). Secondly, at these concentrations $\Gamma_s \approx (\Gamma^{rad}_{Gd} + \Gamma^{Q}_{Gd})$; see equation (14). Since Γ^{Q}_{Gd} is expected to decrease significantly with decreasing temperature, an increase of $Y_{Ce2,s}$ may very well result according to equation (17). Finally, transfer from the higher Gd^{3+} levels to Ce_2^{3+} is expected to be much less dependent on temperature since the spectral overlap is much better.

In contrast with the case of $CsGd_2F_7 : 0.004$ mol% Ce^{3+}, the yield of $CsGd_2F_7 : 10$ mol% Ce^{3+} is almost independent of temperature between 95 and 300 K; see figure 5. This is exactly what is expected since at this concentration $\Gamma_s \approx p_s \Gamma^{rad}_{Ce2}$, so $Y_{Ce2,s} \approx N(0)$ independently of temperature; see equation (17). The decrease of the yield of this sample at high temperatures is ascribed to thermal quenching of the Ce_2^{3+} luminescence.

5. Conclusions

We have shown that VUV excitation and absorption data can yield a lot of information about the processes which are responsible for the scintillation characteristics of a crystal.

In the case of $CsY_2F_7 : Ce^{3+}$ we proved the existence of two inequivalent Ce^{3+} centres, denoted as Ce_1^{3+} and Ce_2^{3+}. We also showed that these are not efficiently excited by the electron–hole pairs created upon absorption of a gamma quantum.

In the case of $CsGd_2F_7 : Ce^{3+}$ the investigation of different energy transfer processes by means of optical excitation allowed us to develop a semiquantitative model which provided correct predictions on the scintillation decay characteristics and photon yield. This model may also be applicable to other luminescence systems in which energy-transfer and migration is important.

As inorganic scintillators for the detection of high-energy gamma particles neither $CsY_2F_7 : Ce^{3+}$ nor $CsGd_2F_7 : Ce^{3+}$ seem very promising. Although the Ce^{3+} $5d \rightarrow 4f$ luminescence in $CsY_2F_7 : Ce^{3+}$ has a rather fast decay time of 32 ns, its light yield is relatively low, as is the density of the host crystal. Since the Ce^{3+} ions are only excited directly in the ionization track of a gamma particle, the light yield is likely to increase at higher Ce^{3+} concentrations. However, concentration quenching due to $Ce_2^{3+} \rightarrow Ce_2^{3+}$

transfer may become important, although the presence of Ce_1^{3+} centres may slow down this transfer, as it enlarges the average distance between Ce_2^{3+} ions.

Both density and light yield of $CsGd_2F_7:Ce^{3+}$ are higher as a result of the presence of Gd^{3+} as a matrix-forming element. However, the decay of the Ce^{3+} luminescence is too slow to be of much practical use, due to the slow population of the Ce_2^{3+} ions via the Gd^{3+} sublattice. The decay will become faster as the Ce^{3+} concentration increases, but at very high Ce^{3+} concentrations energy migration over the Gd^{3+} sublattice will be distorted, and $Ce^{3+} \rightarrow Ce^{3+}$ transfer becomes increasingly important. We are not able to predict what influence this will have on the light yield. However, the light yield of the dominating slow decay component saturates at about 6000 photons MeV^{-1}, which implies that no combination of temperature and Ce^{3+} concentration will lead to a much higher yield for the system $CsGd_2F_7:Ce^{3+}$.

It is clear that the presence of Gd^{3+} as a constituent of the host lattice, which is attractive because of its high atomic number, can have an enormous influence on the scintillation properties of a crystal. If energy migration occurs and transfer to Ce^{3+} ions, or any other dopant, is possible, this will probably result in a higher light yield. Based on the observations made in this work, we note that this will also introduce unwanted slow decay components unless at least the following conditions are fulfilled.

(1) Sufficient spectral overlap must exist between the absorption of the Ce^{3+} ions and all Gd^{3+} levels which lie within the bandgap, so transfer from Gd^{3+} to the Ce^{3+} ions is fast at all Gd^{3+} levels of importance.

(2) Backtransfer from the luminescence centres to the Gd^{3+} ions must be impossible; in the case of Ce^{3+} this means that the relaxed 5d(1) state should be located at longer wavelengths than the Gd^{3+} ^6P level.

(3) The $Gd^{3+} \rightarrow Gd^{3+}$ transfer rates should be high, so that energy migration is fast at all Gd^{3+} levels of importance.

(4) The Ce^{3+} concentration should be high enough to result in a high effective decay rate at all Gd^{3+} levels of importance, although too high a Ce^{3+} concentration may lead to concentration quenching of the Ce^{3+} luminescence.

It is not hard to see that fulfilment of conditions (1) and (2) will be difficult in the case of fluorides since the bandgap energy is relatively high, so the Gd^{3+} ^6P, ^6I, ^6D and ^6I levels all lie within the bandgap. This means that the Ce^{3+} absorption spectrum should at least cover the region from 200 nm to more than 312 nm. In the case of, for example, oxides these conditions are much easier fulfilled since their bandgap is smaller. In this respect we mention the case of $GSO:Ce^{3+}$, in which efficient population of the Ce^{3+} ions via the Gd^{3+} sublattice is reported [15, 16, 17].

Acknowledgments

We wish to thank J T M de Haas for his technical assistance during the experiments.

These investigations were supported by the Netherlands Technology Foundation (STW).

References

[1] van Eijk C W V, Andriessen J, Dorenbos P and Visser R 1994 *Nucl. Instrum. Methods* A **348** 546

[2] Dorenbos P, Visser R, van Eijk C W E, Khaidukov N M and Korzhik M V 1993 *IEEE Trans. Nucl. Sci.* **NS-40** 388

[3] Dorenbos P, Visser R, van Eijk C W E and Khaidukov N M 1993 *Proc. 'Crystal 2000' Int. Workshop on Heavy Scintillators* ed F de Notaristefani, P Lecoq and M Schneegans (Gif-sur-Yvette: Editions Frontières) p 355
[4] Schaart D R, Dorenbos P, van Eijk C W E, Visser R, Pedrini C, Moine B and Khaidukov N M 1995 *Proc. 'Eurodim 94' 7th Europhysical Conf. on Defects in Insulating Materials (Lyon, 1994); Radiat. Effects Defects Solids* **133+134** at press
[5] Pistorius C W F T 1974 *Mater. Res. Bull.* **9** 1337
[6] Ellens A, Kroes S J, Sytsma J, Blasse G and Khaidukov N M 1991 *Mater. Chem. Phys.* **30** 127
[7] Dorenbos P, de Haas J T M, Visser R, van Eijk C W E and Hollander R W 1993 *IEEE Trans. Nucl. Sci.* **NS-40** 424
[8] Samson J A R 1967 *Techniques of Vacuum Ultraviolet Spectroscopy* (New York: Wiley)
[9] Williams R T and Song K S 1990 *J. Phys. Chem. Solids* **51** 679
[10] Casalboni M and Grassano U M 1990 *J. Phys. Chem. Solids* **51** 805
[11] Visser R, Dorenbos P, van Eijk C W E, Meijerink A, Blasse G and den Hartog H W 1993 *J. Phys.: Condens. Matter* **5** 1659
[12] Visser R, Andriessen J, Dorenbos P and van Eijk C W E 1993 *Proc. 'Crystal 2000' Int. Workshop on Heavy Scintillators* ed F de Notaristefani, P Lecoq and M Schneegans (Gif-sur-Yvette: Editions Frontières) p 201
[13] Visser R 1993 Energy transfer in fluoride scintillators *Thesis* Delft University of Technology, The Netherlands
[14] Suzuki H, Tombrello T A, Melcher C L and Schweitzer J S 1993 *IEEE Trans. Nucl. Sci.* **NS-40** 380
[15] Suzuki H, Tombrello T A, Melcher C L and Schweitzer J S 1992 *Nucl. Instrum. Methods.* A **320** 263
[16] Suzuki H, Tombrello T A, Melcher C L and Schweitzer J S 1993 *IEEE Conference Record (San Francisco, CA, 1993)* vol 1, p 14
[17] Suzuki H, Tombrello T A, Melcher C L and Schweitzer J S 1994 *J. Lumin.* **60 & 61** 963
[18] Leskelä M, Saakes M and Blasse G 1984 *Mater. Res. Bull.* **19** 151
[19] Blasse G 1982 *Phys. Status Solidi* a **73** 205
[20] Blasse G 1988 *Prog. Solid State Chem.* **18** 79
[21] Dexter D L 1953 *J. Chem. Phys.* **21** 836